

2,61a

Wicksland

2,61a

ASD-TDR-63-663

DRAG COEFFICIENTS OF SEVERAL BODIES OF REVOLUTION AT TRANSONIC AND SUPERSONIC VELOCITY

TECHNICAL DOCUMENTARY REPORT No. ASD-TDR-63-663

SEPTEMBER 1964

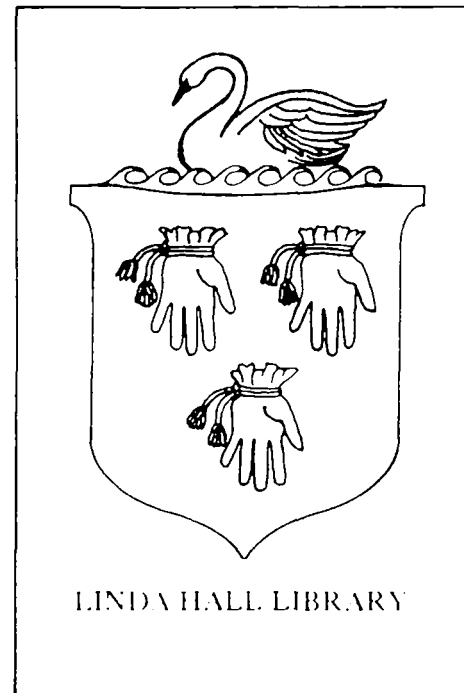
AF FLIGHT DYNAMICS LABORATORY
RESEARCH AND TECHNOLOGY DIVISION
AIR FORCE SYSTEMS COMMAND
WRIGHT-PATTERSON AIR FORCE BASE, OHIO

Project No. 6065, Task No. 606503

(Prepared under Contract No. AF 33(616)-8310 by the
Department of Aeronautics and Engineering Mechanics,
University of Minnesota, Minneapolis, Minnesota;
H. G. Heinrich, Sheldon R. Hess, and Gunar Stumbbris, Authors)

XTL750
.H4414
1964

When Government uses any purpose other than procurement operations, responsibility nor ment may have for drawings, specifications or otherwise as in a corporation, or contract or sell any patent.



other data are used for directly related Government procurement thereby incurs no liability. The fact that the Government supplied the said drawings, regarded by implication or otherwise, or any other person or organization to manufacture, use, or sell any article which may be related thereto.

Qualified requesters may obtain copies of this report from the Defense Documentation Center (DDC), (formerly ASTIA), Cameron Station, Bldg. 5, 5010 Duke Street, Alexandria, Virginia, 22314.

This report has been released to the Office of Technical Services, U.S. Department of Commerce, Washington 25, D. C., in stock quantities for sale to the general public.

Copies of this report should not be returned to the Research and Technology Division, Wright-Patterson Air Force Base, Ohio, unless return is required by security considerations, contractual obligations, or notice on a specific document.

400 - November 1964 - 448-11-302

LINDA HALL LIBRARY



3 3690 00566 1391

FOREWORD

This report was prepared by the Department of Aeronautics and Engineering Mechanics of the University of Minnesota under USAF Contract No. AF 33(616)-8310. This contract was initiated under Project No. 6065, Task No. 606503. The work was administered under the direction of the Recovery and Crew Station Branch, AF Flight Dynamics Laboratory, Research and Technology Division. Mr. Rudi J. Berndt and Mr. James H. DeWeese were the project engineers.

The work accomplished under this contract was sponsored jointly by QM Research and Engineering Command, Department of the Army; Bureau of Aeronautics and Bureau of Ordnance, Department of the Navy; and Air Force Systems Command, Department of the Air Force, and was directed by a Tri-Service Steering Committee concerned with Aerodynamic Retardation.

Individuals who have contributed significantly to the project are: Mr. J. G. Ballinger, Principal Engineer, Rosemount Aeronautical Laboratories, and a number of graduate and undergraduate students of the Institute of Technology of the University of Minnesota.

XTL750

440414
1964

ABSTRACT

The drag coefficients of several bodies of revolution which are significant for the purpose of aerodynamic deceleration were measured in the transonic flow regime and at supersonic speeds of Mach numbers 4 and 5.

This technical documentary report has been reviewed and is approved.

Theron J. Baker
Vehicle Equipment Division
AF Flight Dynamics Laboratory

TABLE OF CONTENTS

<u>Section</u>	<u>Page</u>
I. Introduction	1
II. Models, Facilities, and Instrumentation	2
A. Models	2
B. Wind Tunnels	2
C. Drag Balance	2
D. Flow Visualization	6
E. Pressure Measurements	6
III. Results	7
A. Drag Coefficients at Transonic Speeds	7
B. Drag Coefficients at Supersonic Mach Numbers	9
C. Detailed Discussion of Test Results	9
1. Ogive Cylinder	11
2. Sphere	14
3. Circular Flat Plate	14
IV. Conclusions	18
Appendix I - Representative Flow Photographs .	19
Appendix II - Test Data	31
Appendix III - Description of the Drag Balance System	39
List of References	42

LIST OF ILLUSTRATIONS

<u>Figure No</u>		<u>Page</u>
1.	Wind Tunnel Models (Ogive Cylinder, Skirt Hemisphere, Sphere)	3
2.	Wind Tunnel Models (Cone, Circular Flat Plate, Hollow Hemisphere, Guide Surface Parachute)	4
3.	1.6-inch Diameter Sphere Installed in Transonic Wind Tunnel	5
4.	1.2-inch Diameter Ogive Cylinder Installed in Supersonic Wind Tunnel	5
5.	Drag Coefficients of Several Bodies of Revolution at Transonic Speeds	8
6.	Drag Coefficients at $M_\infty = 4.01$ and 5.01 . . .	10
7.	Variation of Drag Coefficient with Fineness Ratio for Ogive Cylinder at $M_\infty = 2.64$	12
8.	Drag Coefficient of an Ogive Cylinder	13
9.	Drag Coefficient of a Sphere	15
10.	Drag Coefficient of a Circular Flat Plate . .	16
11.	Shadowgraph of 1.2-inch Diameter Ogive Cylinder at $M_\infty = 1.215$; Wake Total Pressure Rake at $X/D = 2.75$	20
12.	Shadowgraph of 1.2-inch Diameter Skirted Hemisphere at $M_\infty = 1.278$	20
13.	Shadowgraph of 1.6-inch Diameter Sphere at $Mach_\infty = 1.217$; Wake Total Pressure Rake at $X/D = 4.5$	21
14.	Shadowgraph of 1.6-inch Diameter 45° Half- Angle Cone at $M_\infty = 1.217$; Wake Total Pressure Rake at $X/D = 4.5$	21
15.	Shadowgraph of 1.6-inch Diameter Circular Flat Plate at $M_\infty = 1.215$ (Head Shock Hidden from View); Wake Total Pressure Rake at $X/D = 4.5$	22

<u>Figure No</u>	<u>Page</u>
16. Shadowgraph of 1.6-inch Diameter Hollow Hemisphere at $M_\infty = 1.210$ (Head Shock Hidden from View); Wake Total Pressure Rake at $X/D = 4.5$	22
17. Shadowgraph of 1.6-inch Diameter Guide Surface Parachute Model at $M_\infty = 1.224$ (Head Shock Hidden from View); Wake Total Pressure Rake at $X/D = 4.5$	23
18. Schlieren Photograph of 1.2-inch Diameter Ogive Cylinder at $M_\infty = 4.01$; Wake Total Pressure Rake at $X/D = 4.5$	23
19. Schlieren Photograph of 1.2-inch Diameter Ogive Cylinder at $M_\infty = 5.01$; Wake Total Pressure Rake at $X/D = 0.5$	24
20. Schlieren Photograph of 0.5625-inch Diameter Skirted Hemisphere at $M_\infty = 4.35$. .	24
21. Schlieren Photograph of 1.6-inch Diameter Sphere at $M_\infty = 4.01$; Wake Total Pressure Rake at $X/D = 2.0$	25
22. Schlieren Photograph of 1.6-inch Diameter Sphere at $M_\infty = 5.01$; Wake Total Pressure Rake at $X/D = 0.5$	25
23. Schlieren Photograph of 1.6-inch Diameter 45° Half-Angle Cone at $M_\infty = 4.01$ (Separated Flow in Base Region); Wake Total Pressure Rake at $X/D = 4.46$	26
24. Schlieren Photograph of 1.6-inch Diameter 45° Half-Angle Cone at $M_\infty = 5.01$; Wake Total Pressure Rake at $X/D = 2.0$	26
25. Schlieren Photograph of 1.6-inch Diameter 45° Half-Angle Cone at $M_\infty = 5.01$ (Separated Flow in Base Region); Wake Total Pressure Rake at $X/D = 2.0$	27
26. Schlieren Photograph of 1.6-inch Diameter Circular Flat Plate at $M_\infty = 4.01$ (Separated Flow in Base Region); Wake Total Pressure Rake at $X/D = 0.5$	27

<u>Figure No</u>	<u>Page</u>
27. Schlieren Photograph of 1.6-inch Diameter Circular Flat Plate at $M_\infty = 5.01$; Wake Total Pressure Rake at $X/D = 0.5$	28
28. Schlieren Photograph of 1.6-inch Diameter Hollow Hemisphere at $M_\infty = 4.01$; Wake Total Pressure Rake at $X/D = 2.0$	28
29. Schlieren Photograph of 1.6-inch Diameter Hollow Hemisphere at $M_\infty = 5.01$; Wake Total Pressure Rake at $X/D = 0.5$	29
30. Schlieren Photograph of 1.6-inch Diameter Guide Surface Parachute Model at $M_\infty = 4.01$ (Separated Flow in Base Region); Wake Total Pressure Rake at $X/D = 0.5$	29
31. Schlieren Photograph of 1.6-inch Diameter Guide Surface Parachute Model at $M_\infty = 5.01$; Wake Total Pressure Rake at $X/D = 0.5$	30
32. Variation of Drag Coefficient of Ogive Cylinder with Freestream Mach Number	32
33. Variation of Drag Coefficient of Skirted Hemisphere with Freestream Mach Number	33
34. Variation of Drag Coefficient of Sphere with Freestream Mach Number	34
35. Variation of Drag Coefficient of 45° Half-Angle Cone with Freestream Mach Number	35
36. Variation of Drag Coefficient of Circular Flat Plate with Freestream Mach Number	36
37. Variation of Drag Coefficient of Hollow Hemisphere with Freestream Mach Number	37
38. Variation of Drag Coefficient of Guide Surface Parachute Model with Freestream Mach Number	38
39. Drag Balance (Photograph)	40

LIST OF SYMBOLS

C_D	= drag/ $q_\infty S$ S = drag coefficient
S	= projected area, $D^2\pi/4$
D	= maximum body diameter
L	= overall body length
L/D	= body fineness ratio
M_∞	= freestream Mach number
P_0	= wind tunnel stagnation pressure
q_∞	= freestream dynamic pressure
Re	= $\rho VD/\mu$ = Reynolds number (based on maximum body diameter)
X	= distance downstream from body base

I. INTRODUCTION

Numerous investigations of the aerodynamic drag of relatively slender, low drag bodies have been conducted, but little information is available on the drag characteristics of relatively blunt bodies. In problems of aerodynamic deceleration, however, the blunt, high drag bodies are very important. Knowledge of their drag characteristics is especially necessary when their application as decelerators for other bodies is considered.

Therefore, a study is being made at the University of Minnesota whose overall objective has been identified as: "Investigation of Wake Effects on the Behavior of Parachutes and Other Retardation Devices Behind Large Bodies of Revolution at Subsonic and Supersonic Speeds." To investigate these wake effects it is necessary to know the drag characteristics of the related bodies in undisturbed flow. Since such knowledge is not generally available, a series of tests was conducted as part of the general program to determine the freestream drag characteristics of the various bodies. This report presents the results of these tests in the transonic and supersonic flow regimes, while similar results for subsonic flow are given in Ref 1.

Manuscript released by the authors August 1962 for publication as an ASD Technical Documentary Report.

II. MODELS, FACILITIES, AND INSTRUMENTATION

A. Models

The following seven bodies were included in the test program:

- A. Ogive cylinder (2.5 caliber tangent nose, fineness ratio = 4.5)
- B. Skirted hemisphere
- C. Sphere
- D. 45° half-angle cone
- E. Circular flat plate
- F. Hollow hemisphere
- G. Guide surface parachute model

The general shapes and dimensions of these seven bodies are shown in Figs 1 and 2.

B. Wind Tunnels

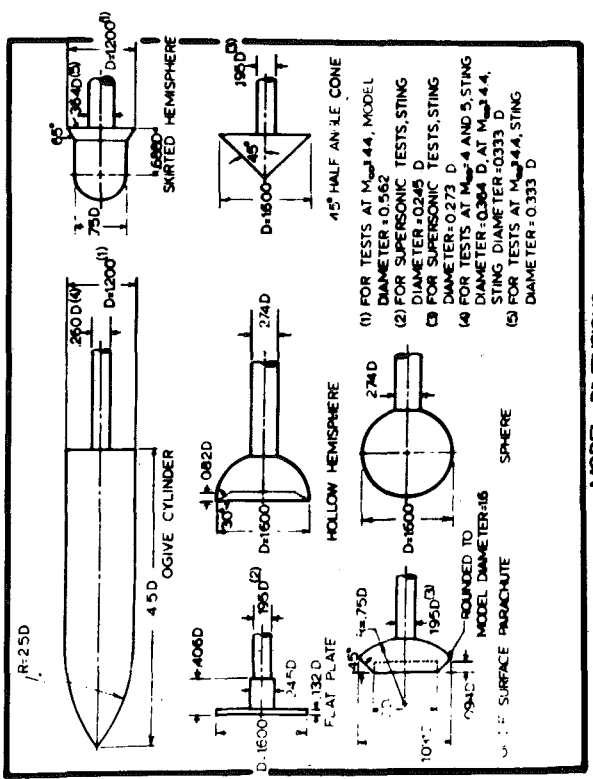
The tests were conducted in the wind tunnels of Rosemount Aeronautical Laboratories. Transonic tests were made in the 12 x 16 inch continuous flow, induction type wind tunnel. Supersonic experiments were conducted in the 6 x 9 inch continuous flow supersonic wind tunnels. Detailed descriptions of these facilities are presented in Ref 2.

Typical model installations in the transonic and supersonic tunnels are shown in Figs 3 and 4 respectively. The enlarged portion of the model support sting which can be seen in these photos houses the drag balance.

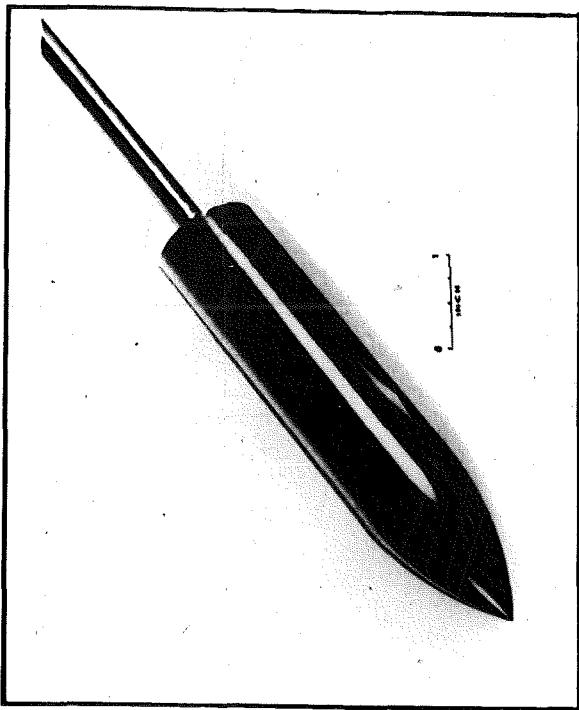
To reduce the total number of tests needed in the overall program, a pressure survey of the wake regions of the various bodies was combined with the drag measurements. Therefore, a total pressure rake was located at various downstream positions (as shown in Figs 3 and 4) in almost all drag tests.

C. Drag Balance

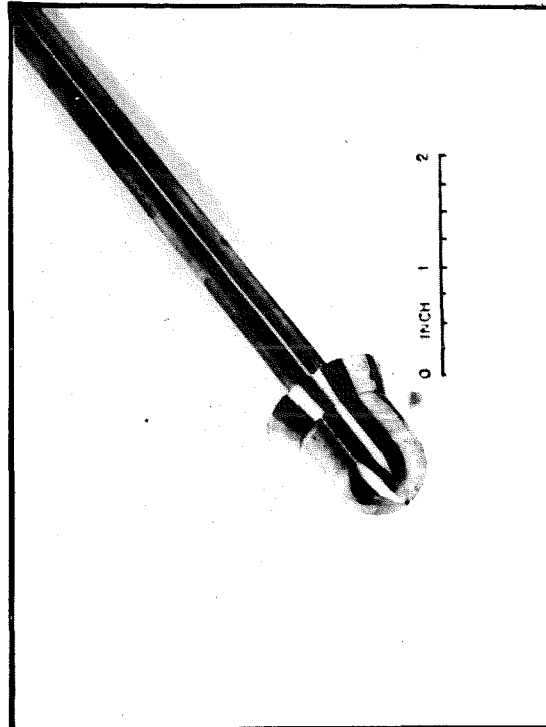
The drag balance used for these tests is a mechanical-



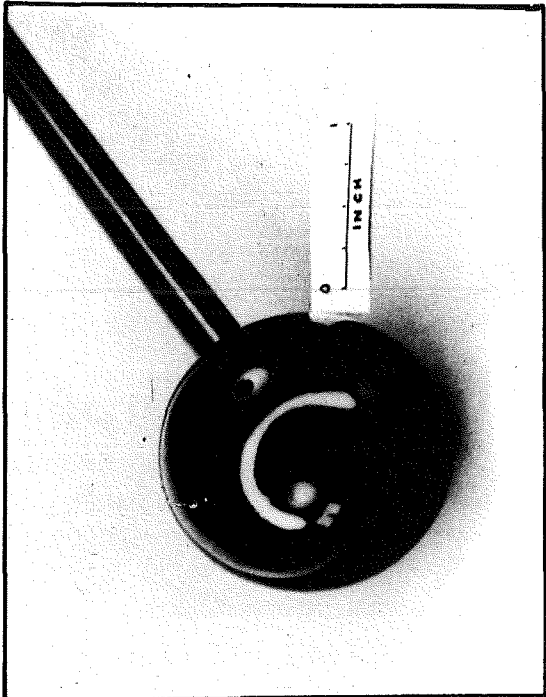
MODEL DIMENSIONS



1.2 INCH DIAMETER OGIVE CYLINDER



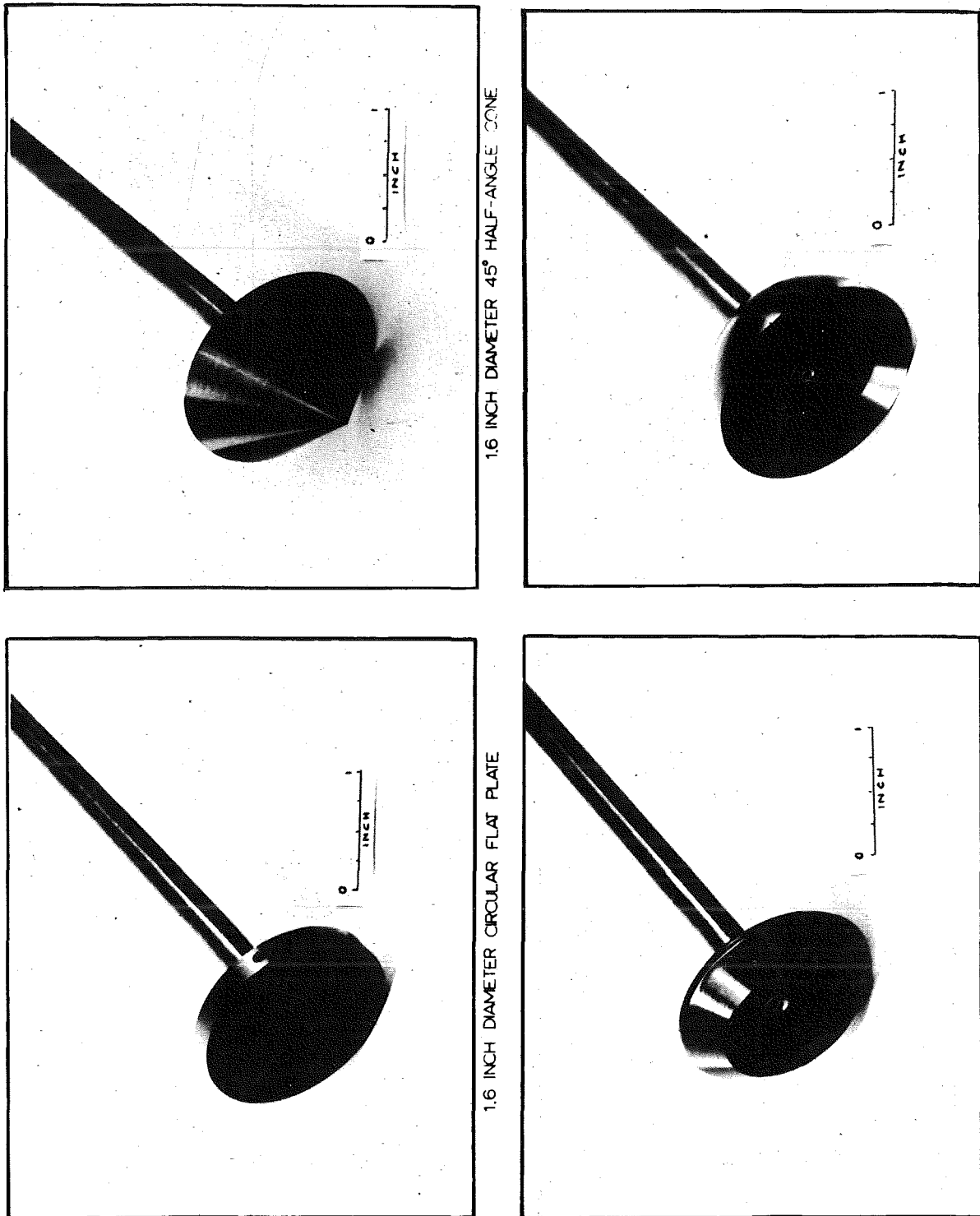
1.2 INCH DIAMETER SKIRTED HEMISPHERE



1.6 INCH DIAMETER SPHERE

FIG. 1. WIND TUNNEL MODELS

FIG 2. WIND TUNNEL MODELS



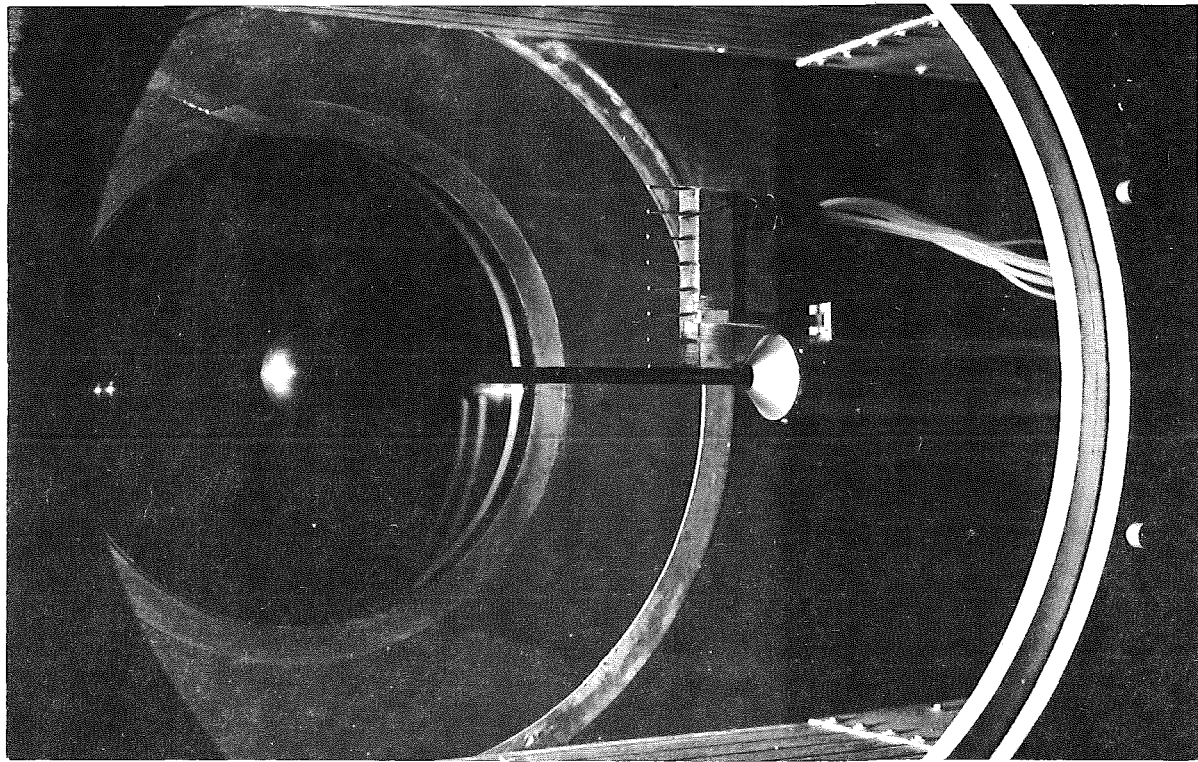


FIG 3. 1.6 INCH DIAMETER SPHERE INSTALLED IN TRANSONIC WIND TUNNEL.

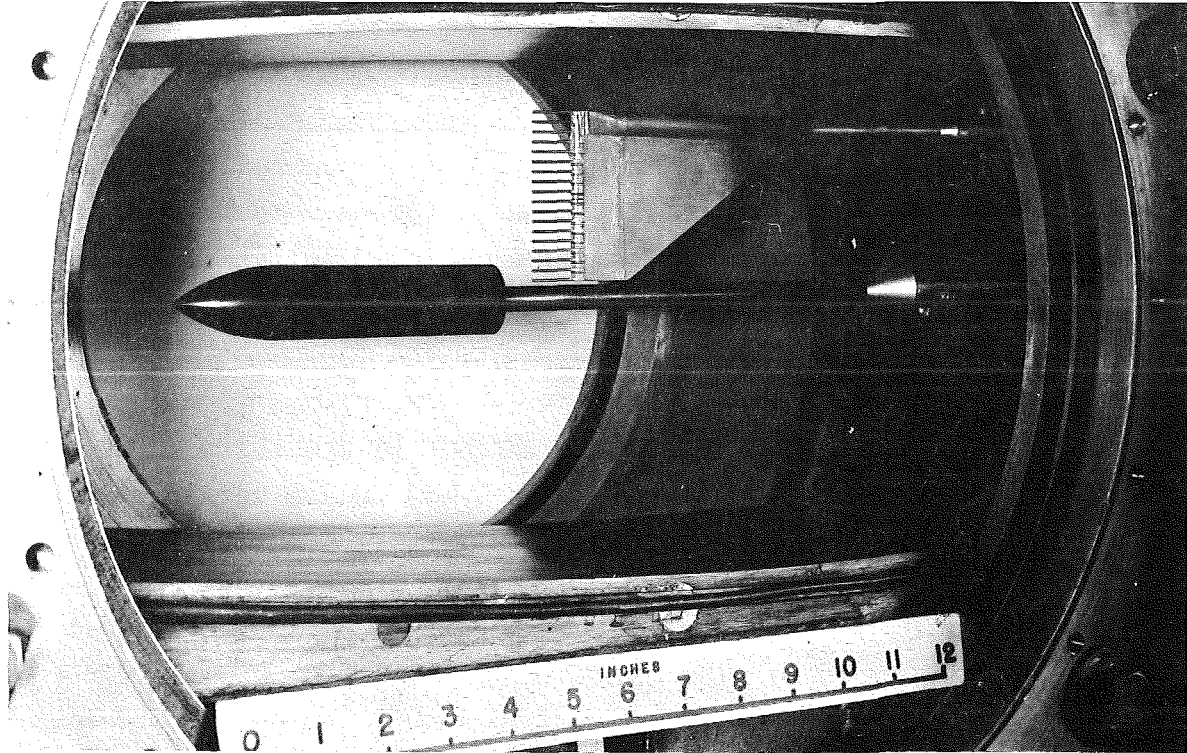


FIG 4. 1.2 INCH DIAMETER OGIVE CYLINDER INSTALLED IN SUPERSONIC WIND TUNNEL.

electrical system whose sensing unit is mounted co-axially with the model support sting. The drag force acts over the support sting upon a pair of flexible steel diaphragms. The deflection of these diaphragms is transmitted to the core of a Schaevitz Linear Variable Differential Transformer (LVDT) which thus gives an electrical signal proportional to the drag on the model. The output of the LVDT is transmitted through a control unit to a Brown Variable Span Recorder which gives a permanent, easily read record of the drag values. A detailed description of the drag balance is given in Appendix III.

D. Flow Visualization

Observations and recording of flow characteristics around test models was accomplished by means of shadowgraph and Schlieren for transonic and supersonic experiments respectively.

E. Pressure Measurement

To correct the measured drag values for the presence of the sting at the base of the body, the body base pressure and the drag balance internal pressure were recorded. The base pressure was determined from base pressure coefficients which were measured by means of the wake total pressure rake. The exception was the skirted hemisphere model which had a base pressure tap. The balance internal pressure was measured directly through an orifice provided for this purpose within the balance.

The pressure taps were connected by plastic tubing to Mercury or merriam fluid (sp. g. = 1.05) manometer boards, which were photographed at each test condition.

III. RESULTS

The objective of this study was the establishment of the drag coefficients of the bodies shown in Fig 1 in the transonic and supersonic flow regime. In addition, representative flow pictures were to be obtained either by the Schlieren or shadowgraph method. The drag coefficients will be discussed in detail in the following pages, whereas the pertinent flow pictures can be found in Appendix I.

The drag measurements and the flow visualization were made at the following approximate Mach numbers: 0.6, 0.85, 0.95, 1.05, 1.2, 4.0, and 5.0. A secondary objective of this study was the establishment of the wake boundaries of the various bodies. For this purpose, a total pressure rake was placed behind the bodies under investigation. In the interest of the wake investigation the rake had to be placed quite close to the body in several instances, and there is certainly the possibility that the rake influenced the drag coefficient of the body. In cases where such a doubt or possibility existed or appeared likely, the drag coefficients have been omitted.

A. Drag Coefficients at Transonic Speeds

Figure 5 presents the results of the measurements on all bodies in the transonic flow regime. The curves show a somewhat regular and expected characteristic with the exception of the drag coefficient of the sphere. In the case of the sphere a strong Reynolds number influence has been noticed at $M_\infty = 0.6$, details of which are discussed later and are illustrated in Fig 9.

More experimental data for the individual bodies are shown in Figs 32 through 38, Appendix II. These figures also show experimental points obtained in the supersonic flow regime.

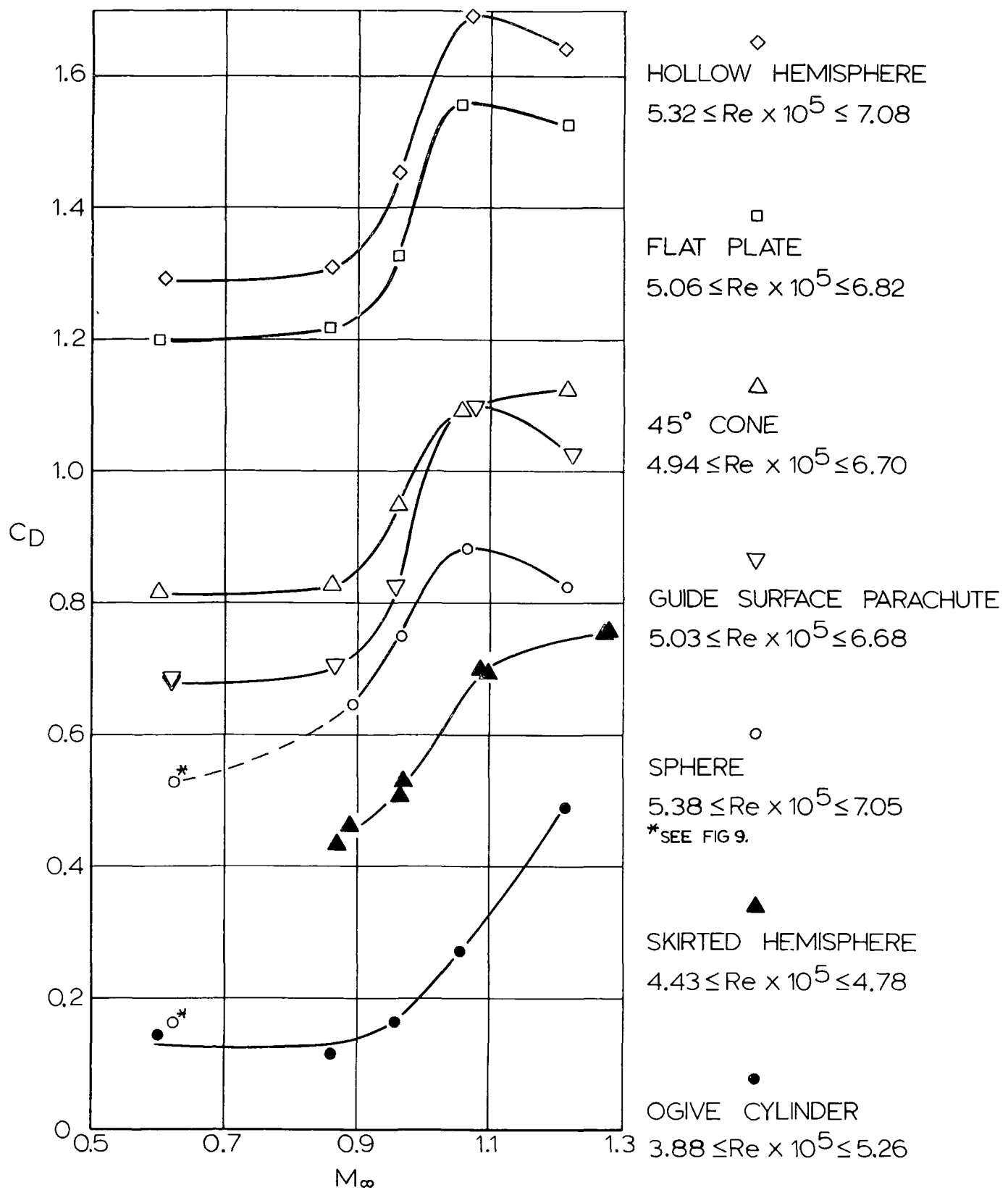


FIG 5. DRAG COEFFICIENTS OF SEVERAL BODIES OF REVOLUTION AT TRANSONIC SPEEDS

B. Drag Coefficients at Supersonic Mach Numbers

The results of measurements in the supersonic flow regime are shown in Fig 6. The indicated points are the results of an averaging process of a continuous force recording obtained from the electric balance.

Figure 6 also indicates the specific location of the total pressure rake and the form of the wake boundary, either converging or diverging.

As can be seen from Fig 6, the location of the total pressure rake appears to be immaterial in view of the drag coefficient, whereas the effect of a converging or diverging wake boundary appears to be more important. For example, the 45° half angle cone is shown in Figs 24 and 25, with converging and diverging wake boundaries. This may be a Reynolds number effect because the Reynolds numbers for Figs 24 and 25 are 8.3×10^5 and 5.8×10^5 respectively. This rake condition accounts for the deviation of the drag coefficients in the order of 10% as can be seen for the 45° half-angle cone at $M_\infty = 5$ in Fig 6.

In view of these experimental circumstances and under consideration of information found in literature, an attempt has been made to establish a drag coefficient of the seven bodies under investigation, which is considered to be fairly reliable. These drag coefficients at $M_\infty = 5$ and their source of information are summarized in Table 1. As can be concluded from Fig 6, the drag coefficients at $M_\infty = 4$ will vary from those at $M_\infty = 5$ depending on the body.

C. Detailed Discussion of Test Results

Very limited information was found in literature on the drag characteristics of the skirted hemisphere, 45° half angle cone, hollow hemisphere, and shapes resembling the guide surface parachute in the transonic and supersonic flow regimes. Therefore, the following comparisons are restricted to a discussion of the ogive cylinder, the sphere, and the flat plate.

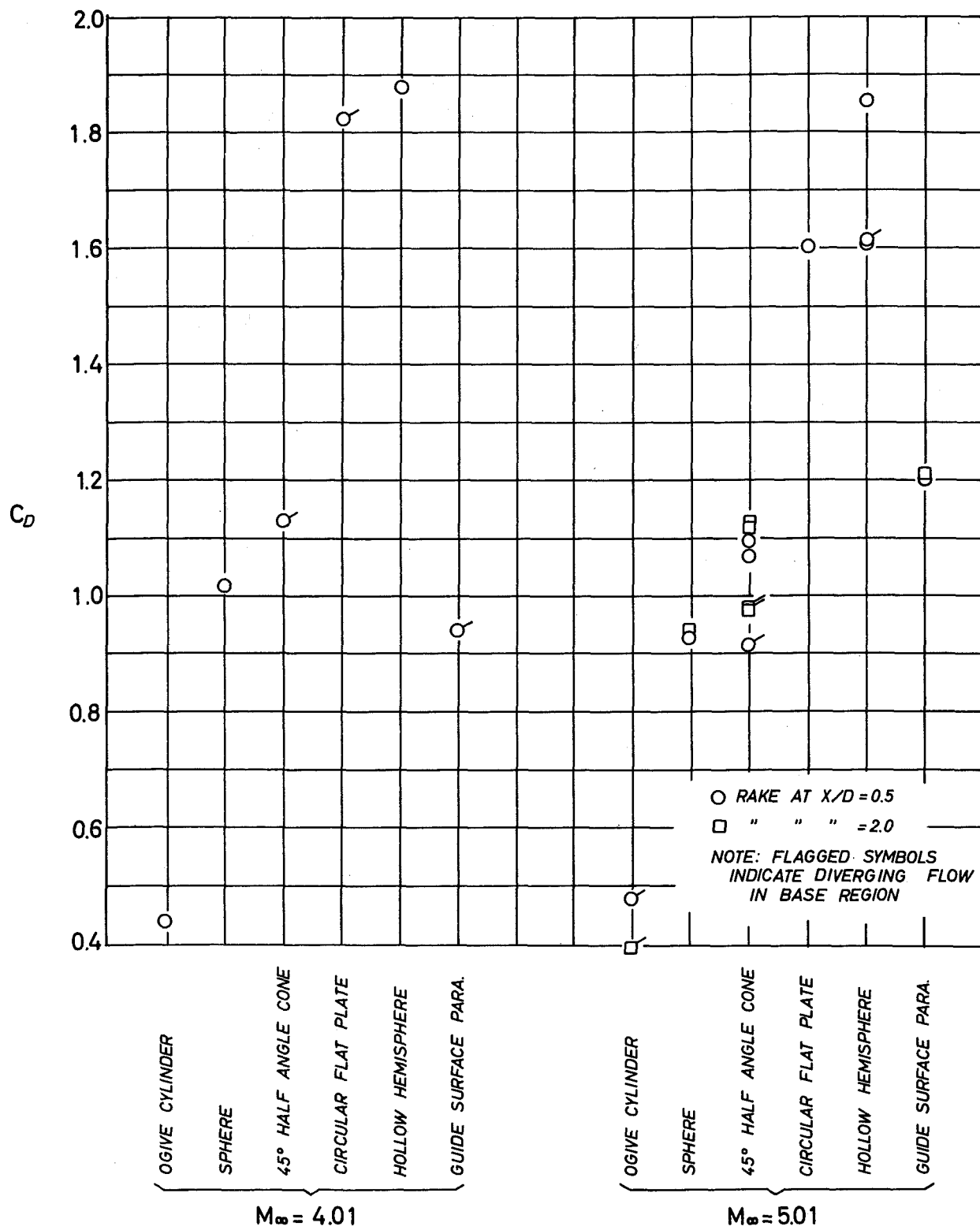


FIG 6. DRAG COEFFICIENTS AT $M_\infty = 4.01$ AND 5.01

TABLE 1. DRAG COEFFICIENT AT $M_\infty = 5$

BODY	C_D	SOURCE
OGIVE CYLINDER	~ 0.4	PRESENT TESTS AND EXTENSION OF RESULTS FROM REFS 14 & 15 (FIG 8)
SKIRTED HEMISPHERE	0.75 (AT $M_\infty = 4.4$)	PRESENT TESTS (FIG 33)
SPHERE	0.93	PRESENT TESTS AND REF 3 (FIG 9)
45° HALF-ANGLE CONE	1.1	PRESENT TESTS (FIG 6)
CIRCULAR FLAT PLATE	1.6	PRESENT TESTS AND REF 3 (FIG 10)
HOLLOW HEMISPHERE	~ 1.7	PRESENT TESTS (FIG 6)
GUIDE SURFACE PARACHUTE MODEL	1.2	PRESENT TESTS (FIG 6)

1. Ogive Cylinder

Most of the results found for similar ogive cylinders were for supersonic Mach numbers between 1.2 and 3.5; no comparable results for this body could be found for the transonic Mach number range.

References 14 and 15 each give drag coefficients for supersonic Mach numbers for ogive cylinders which are very similar to the one used in this investigation. In each case the shape of the ogival nose was the same and the body fineness ratio, L/D , varied by only $\pm \frac{1}{2}$. Based on the results shown in Fig 7, which was extracted from Ref 14, the difference in fineness ratio in this range does not affect the C_D values. This body, however, has a much sharper nose than the one under present investigation.

The results of the present study and the drag coefficients from Refs 14 and 15 are presented in Fig 8. The transonic results from present tests join the results from Refs 14 and 15 in a satisfactory manner, and therefore are acceptable. The supersonic results, however, indicate a slightly higher drag coefficient. Drag coefficients given in Ref 3 for various projectile bodies indicate that no

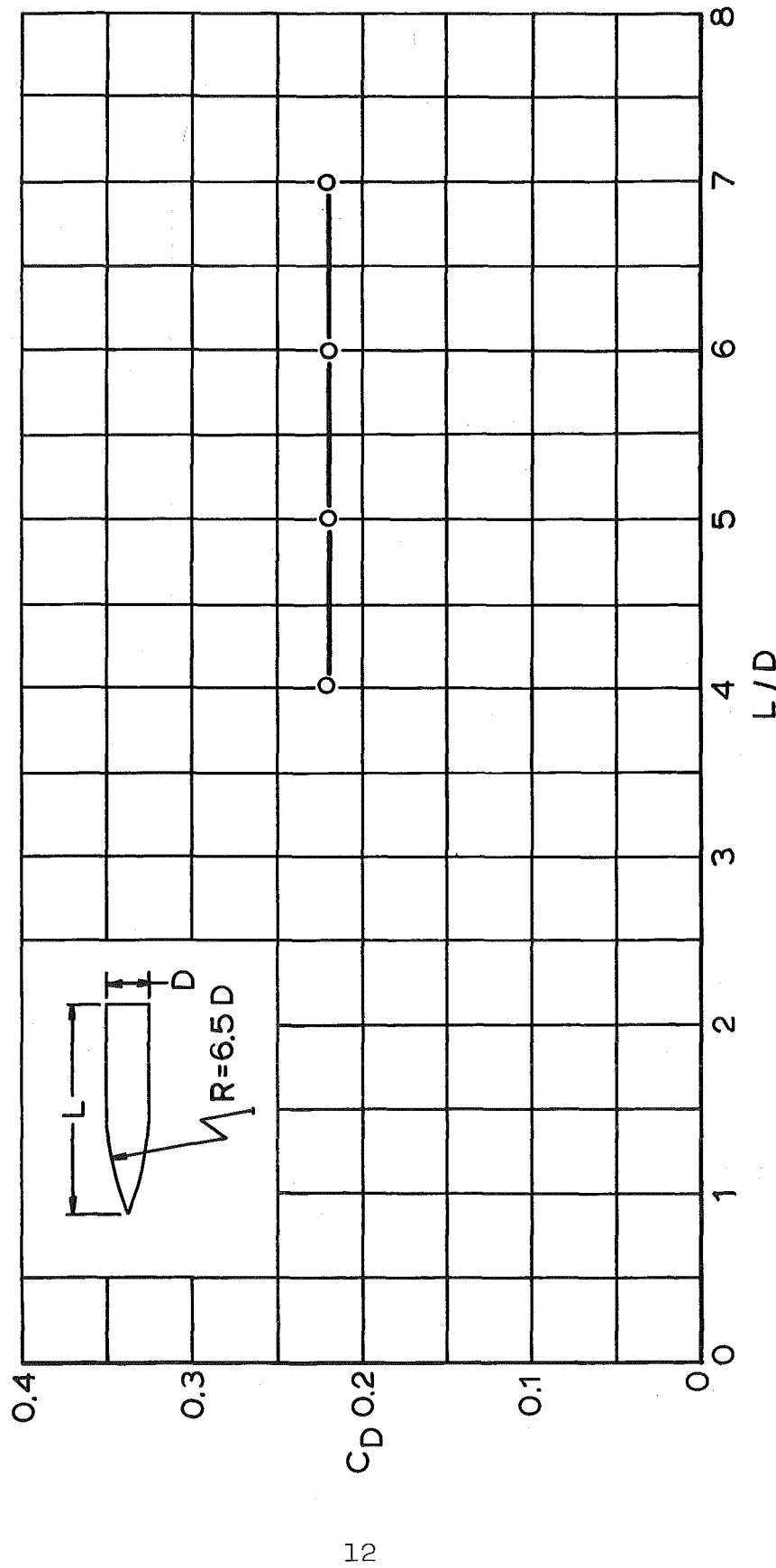


FIG 7. VARIATION OF DRAG COEFFICIENT WITH
FINENESS RATIO FOR OGIVE CYLINDER
AT $M_\infty = 2.64$
(FROM REF 14)

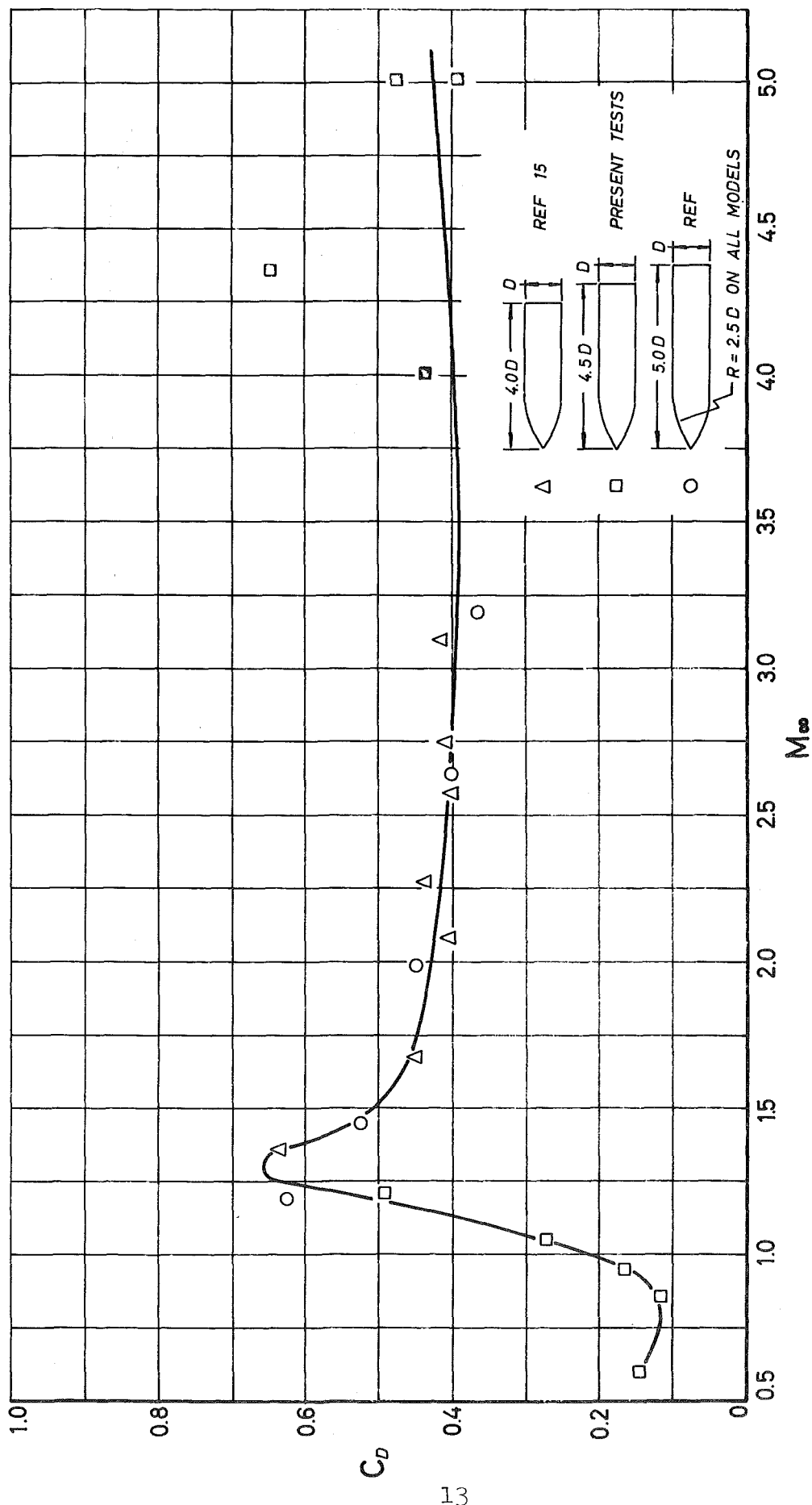


FIG 8. DRAG COEFFICIENTS OF AN OGIVE CYLINDER

significant increase in drag coefficient at these Mach numbers should be expected.

In view of the new results as well as on the basis of information obtained from publications, one would expect C_D values at $M_\infty = 4$ and 5 in the order of 0.4 or slightly below.

2. Sphere

The results of many investigations concerning the drag characteristics of spheres have been summarized in Ref 3. The curve which is presented there for the variation of C_D with M_∞ is reproduced in Fig 9 together with the results from present tests. It is noted that for Mach numbers less than 0.75, the drag curve has two distinctly separate branches. The lower branch is for Reynolds numbers above critical conditions while the upper one is for those below the critical Reynolds number.

The transonic drag coefficient values obtained for the 1.6-inch diameter sphere tested here agree very well with the results from Ref 3, except at $M_\infty = 1.2$. It is noted that the C_D value at $M_\infty = 0.625$ falls on the lower branch of the C_D curve. The Reynolds number for this test was 5.4×10^5 , which is above the critical value. The obtained drag coefficients agree, in general, satisfactorily with those found in other publications.

3. Circular Flat Plate

Only a relatively few experimental values for the drag coefficient of the circular flat plate are available, with none available in the transonic Mach number range. The solid part of the C_D versus M_∞ curve shown in Fig 10 is identical with a pertinent curve given in Ref 3. The transonic section of this curve which is broken, is suggested in consideration of the results obtained in this study.

The drag coefficient value at $M_\infty = 5$ agrees with the results from Ref 3. The test point at $M_\infty = 4$ should be

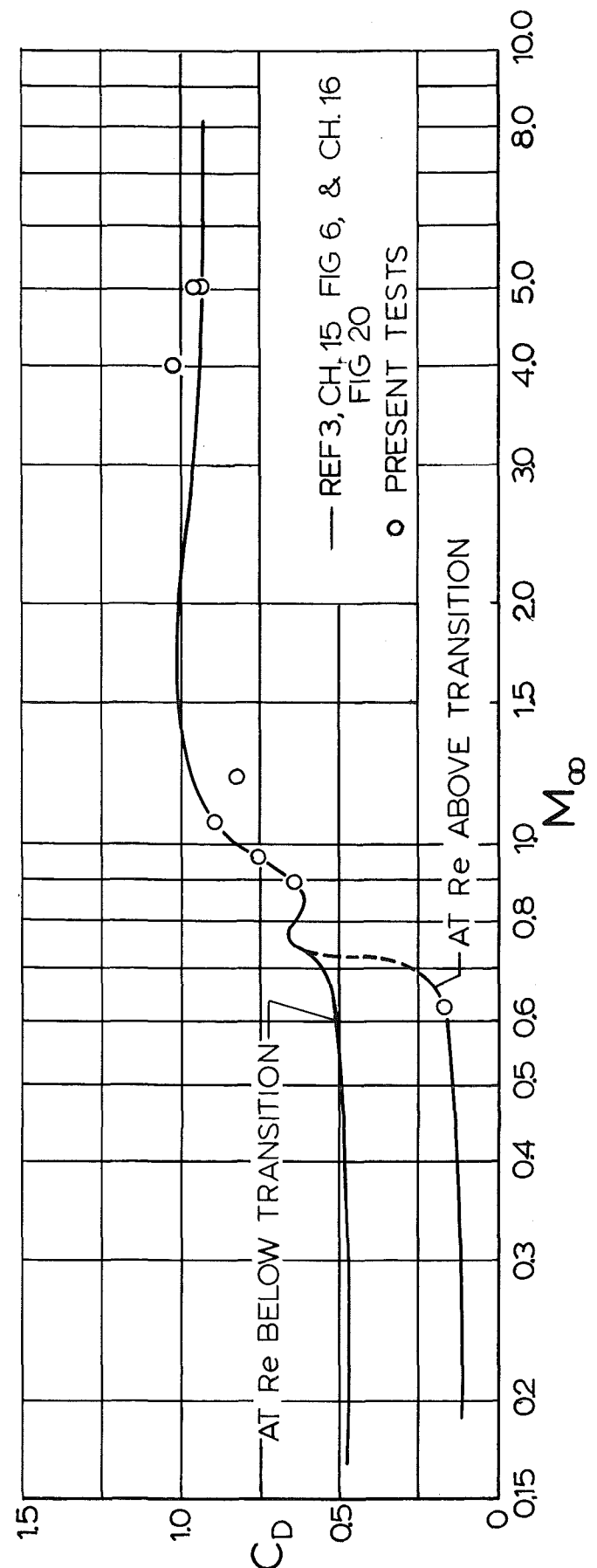


FIG 9. DRAG COEFFICIENT OF A SPHERE

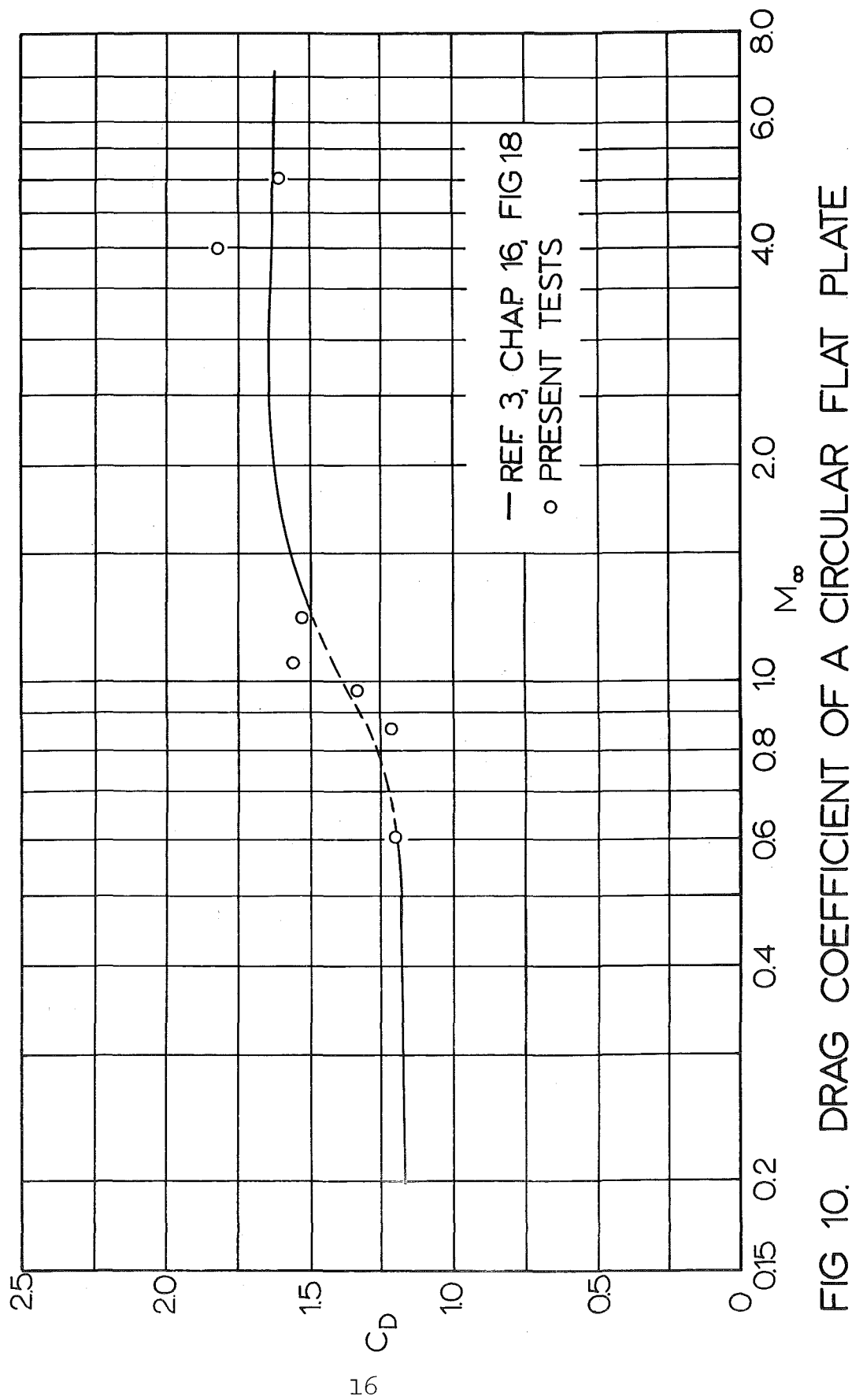


FIG 10. DRAG COEFFICIENT OF A CIRCULAR FLAT PLATE

disregarded because it is known that under these specific experimental conditions, the form of the wake in the near base region was divergent.

IV. CONCLUSIONS

The drag coefficients measured at transonic speeds for the ogive cylinder, skirted hemisphere, sphere, 45° half-angle cone, circular flat, hollow hemisphere and guide surface parachute model are given in Fig 5.

Under consideration of information found in other publications, the most probable drag coefficients for the seven bodies involved in this study at a Mach number of 5 are presented in Table 1. It may be assumed that the drag coefficients related to Mach numbers between the transonic region and the indicated supersonic Mach number will leave values as indicated in the respective curves.

APPENDIX I
REPRESENTATIVE FLOW PHOTOGRAPHS

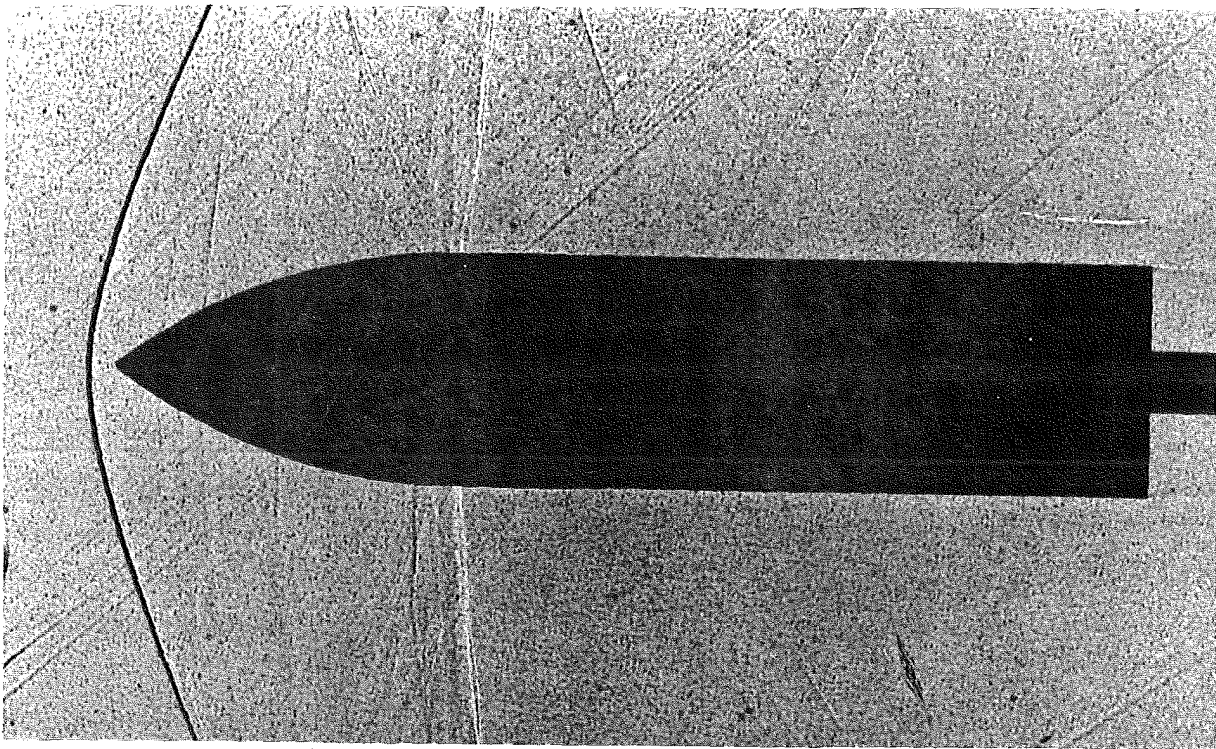


FIG 11. SHADOWGRAPH OF 1.2 INCH DIAMETER OGIVE CYLINDER AT
 $M_{\infty} = 1.215$; WAKE TOTAL PRESSURE RAKE AT $X/D = 2.75$.

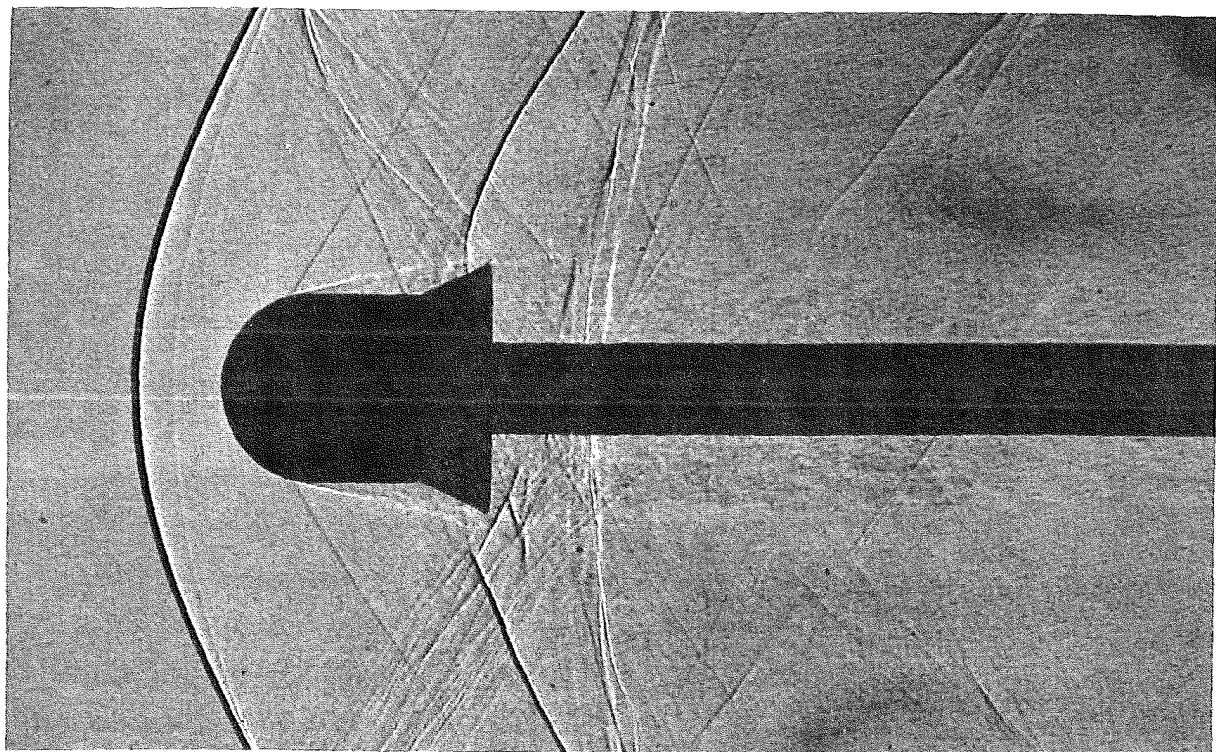


FIG 12. SHADOWGRAPH OF 1.2 INCH DIAMETER SKIRTED HEMISPHERE
AT $M_{\infty} = 1.278$.

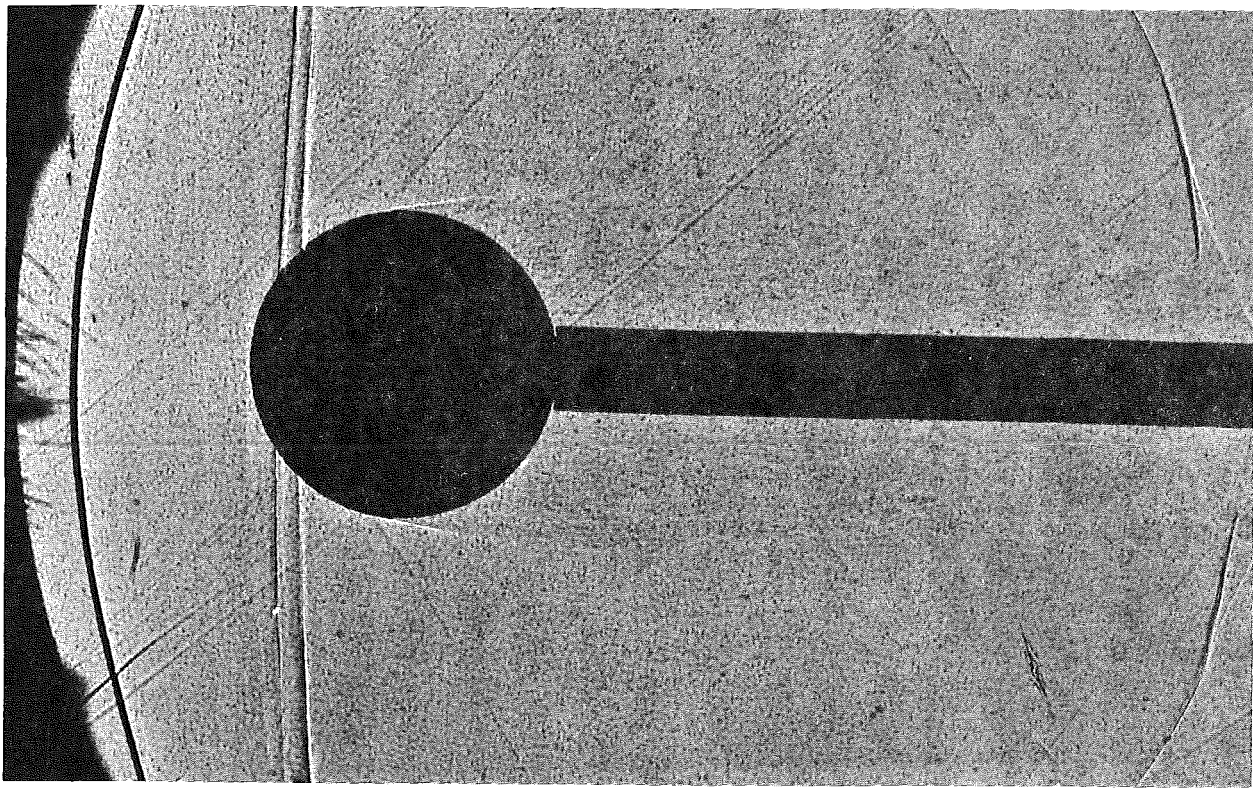


FIG 13. SHADOWGRAPH OF 1.6 INCH DIAMETER SPHERE AT $M_{\infty} = 1.217$; WAKE TOTAL PRESSURE RAKE AT $X/D = 4.5$.

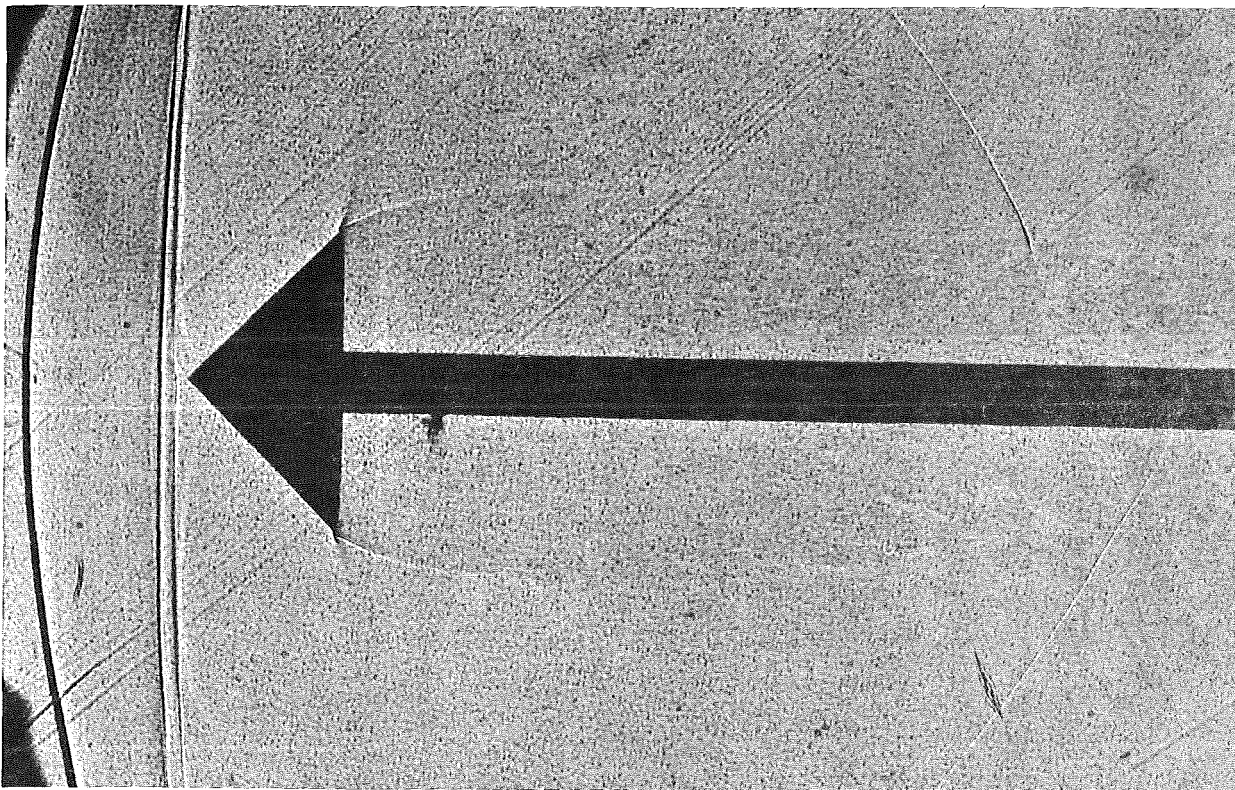


FIG 14. SHADOWGRAPH OF 1.6 INCH DIAMETER 45° HALF-ANGLE CONE AT $M_{\infty} = 1.217$; WAKE TOTAL PRESSURE RAKE AT $X/D = 4.5$.

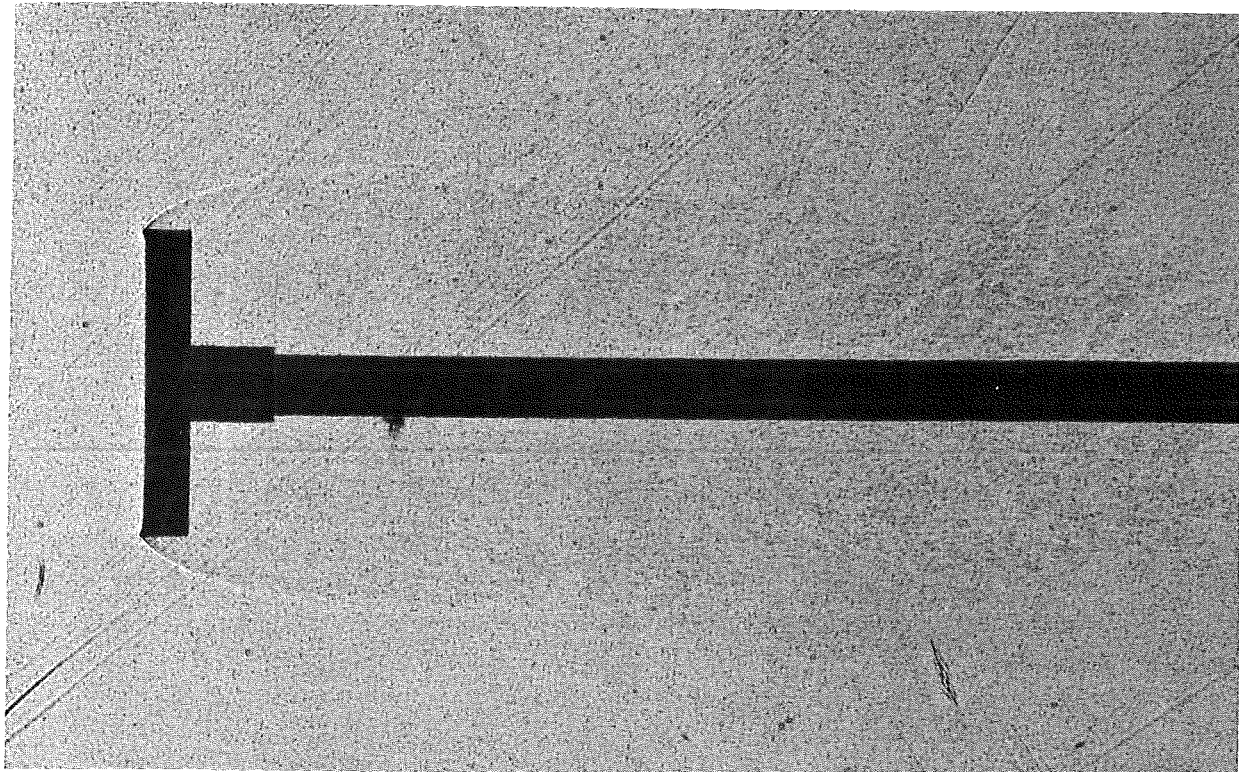


FIG 15. SHADOWGRAPH OF 1.6 INCH DIAMETER CIRCULAR FLAT PLATE
AT $M_{\infty} = 1.215$ (HEAD SHOCK HIDDEN FROM VIEW); WAKE
TOTAL PRESSURE RAKE AT $X/D = 4.5$.

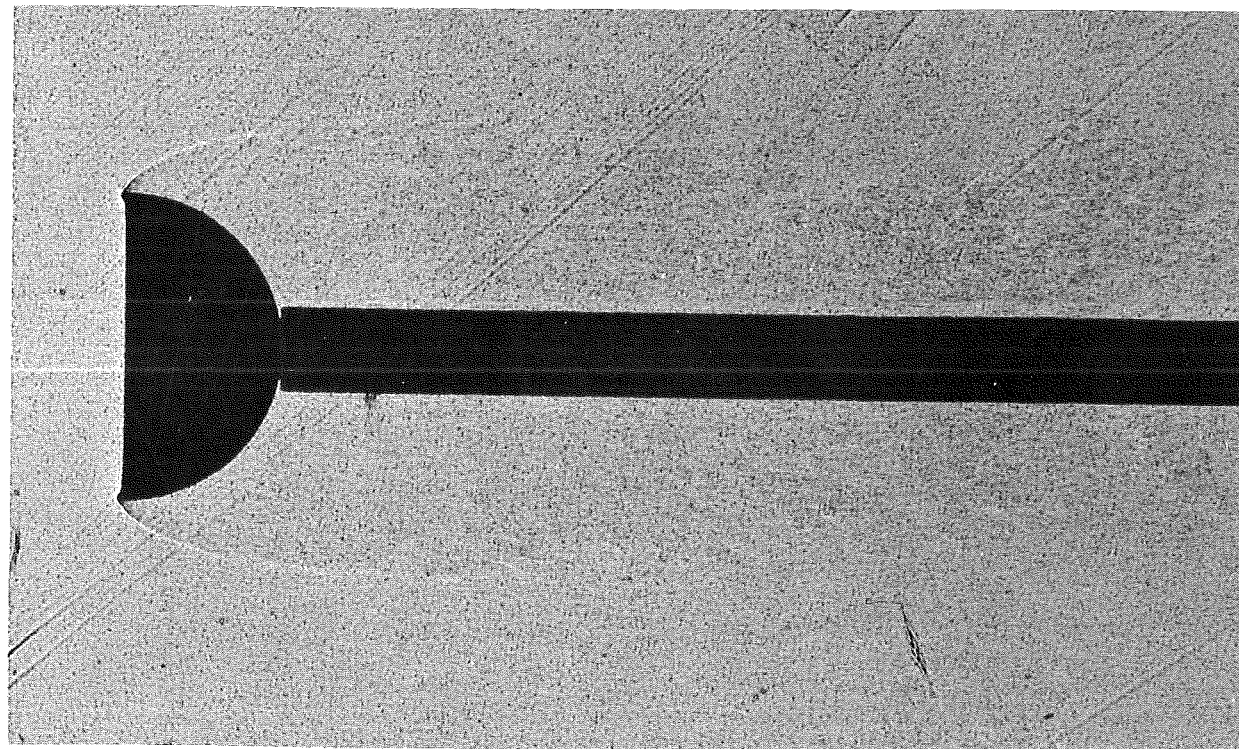


FIG 16. SHADOWGRAPH OF 1.6 INCH DIAMETER HOLLOW HEMISPHERE
AT $M_{\infty} = 1.210$ (HEAD SHOCK HIDDEN FROM VIEW); WAKE
TOTAL PRESSURE RAKE AT $X/D = 4.5$.

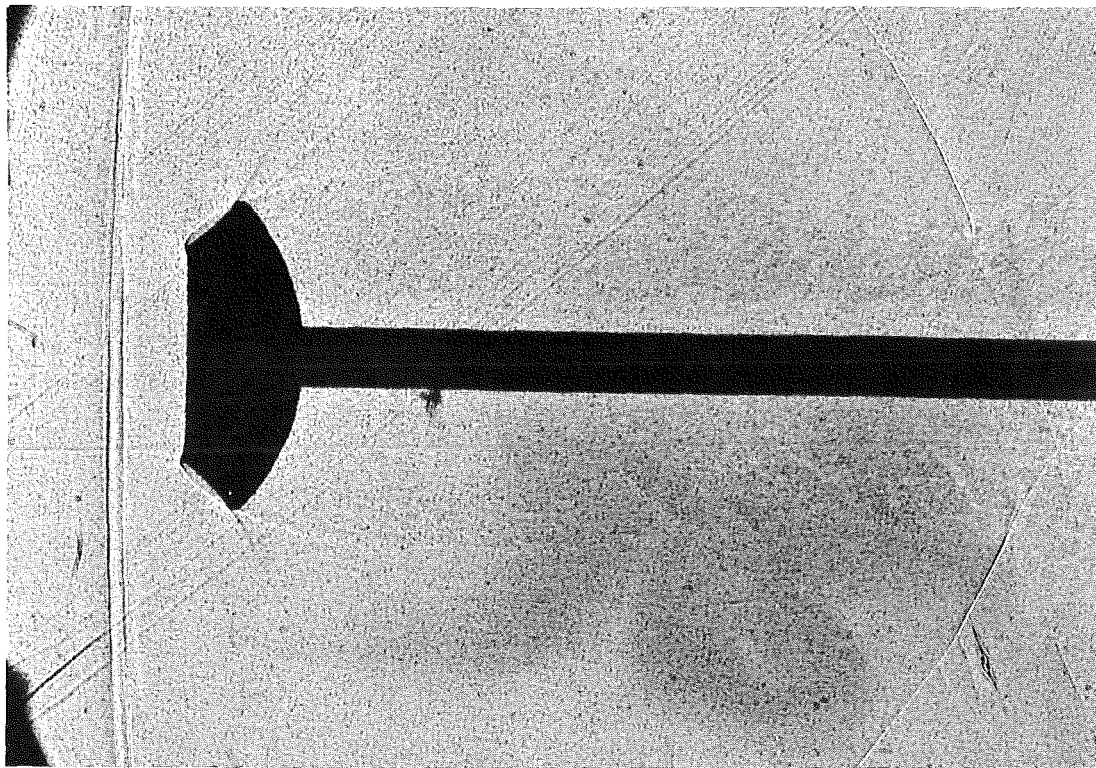


FIG 17. SHADOWGRAPH OF 1.6 INCH DIAMETER GUIDE SURFACE PARACHUTE MODEL AT $M_\infty = 1.224$ (HEAD SHOCK HIDDEN FROM VIEW); WAKE TOTAL PRESSURE RAKE AT $X/D = 4.5$.

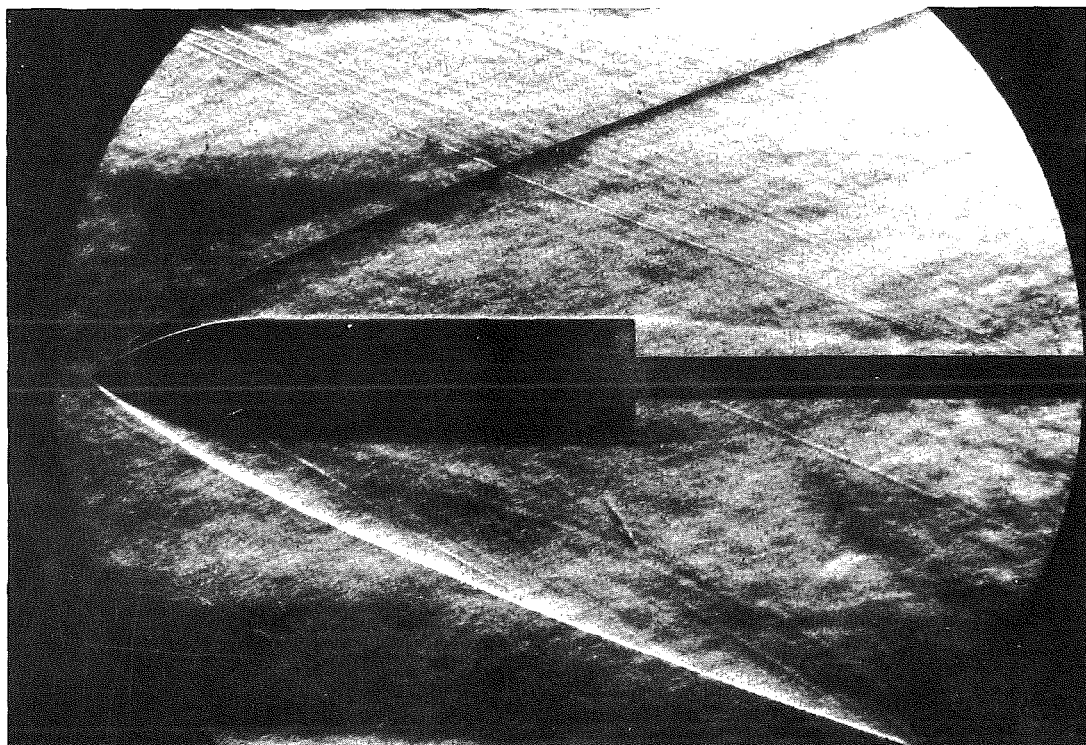


FIG 18. SCHLIEREN PHOTOGRAPH OF 1.2 INCH DIAMETER OGIVE CYLINDER AT $M_\infty = 4.01$; WAKE TOTAL PRESSURE RAKE AT $X/D = 4.5$.

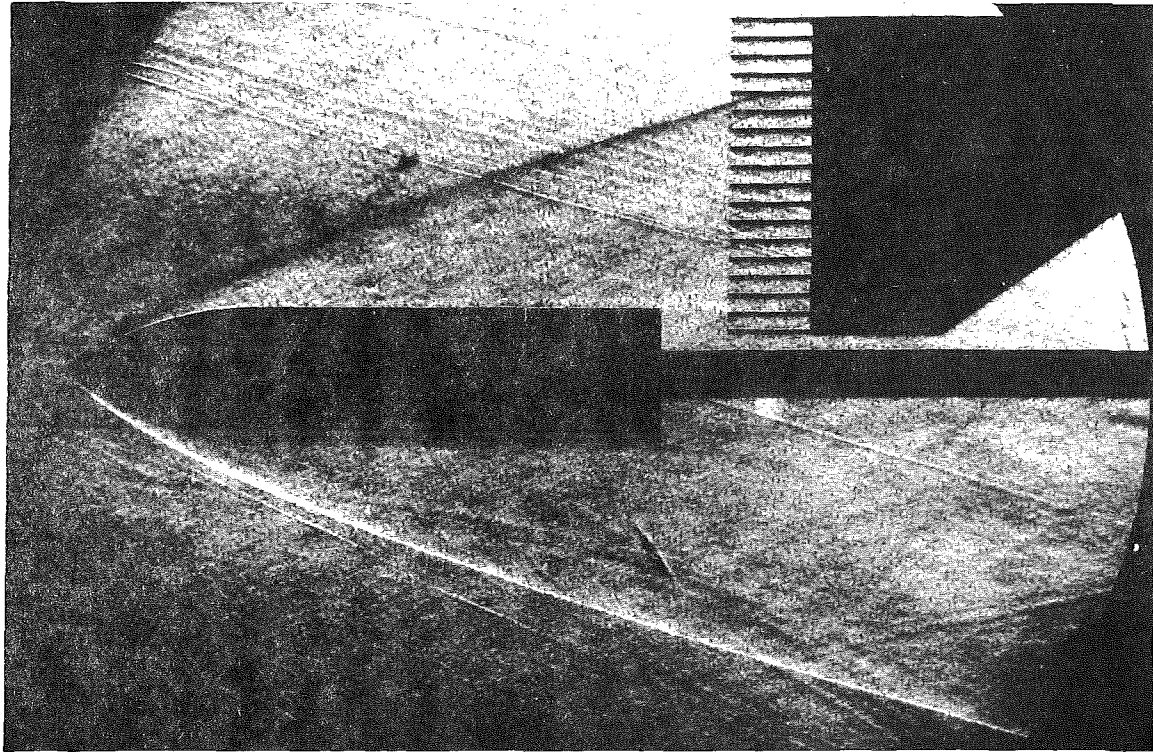


FIG 19. SCHLIEREN PHOTOGRAPH OF 1.2 INCH DIAMETER OGIVE CYLINDER AT $M_{\infty} = 5.01$; WAKE TOTAL PRESSURE RAKE AT $X/D = 0.5$.

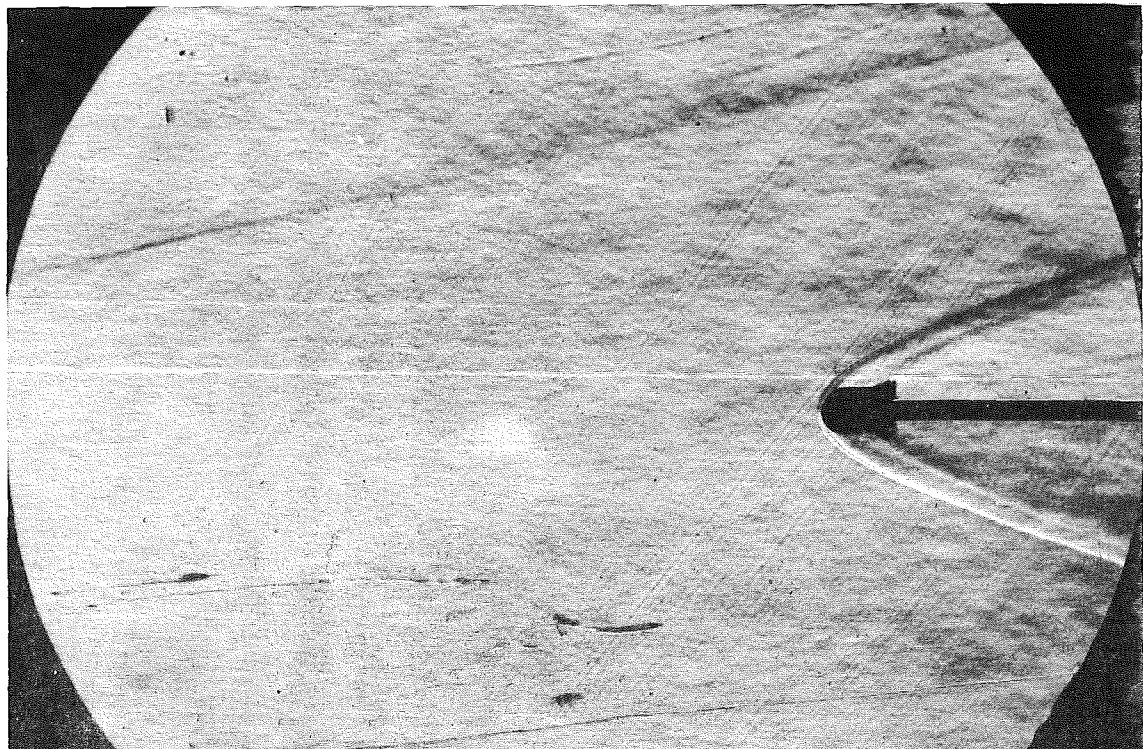


FIG 20. SCHLIEREN PHOTOGRAPH OF 0.5625 INCH DIAMETER SKIRTED HEMISPHERE AT $M_{\infty} = 4.35$.

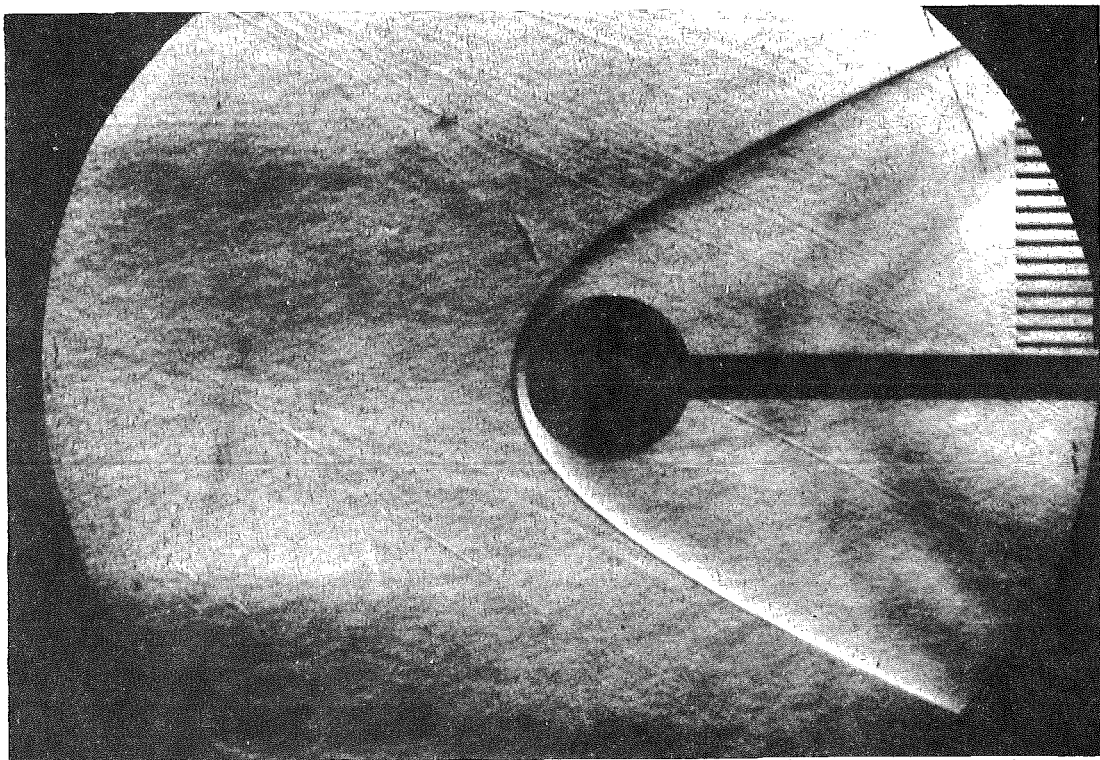


FIG 21. SCHLIEREN PHOTOGRAPH OF 1.6 INCH DIAMETER SPHERE
AT $M_{\infty} = 4.01$; WAKE TOTAL PRESSURE RAKE AT $X/D = 2.0$.

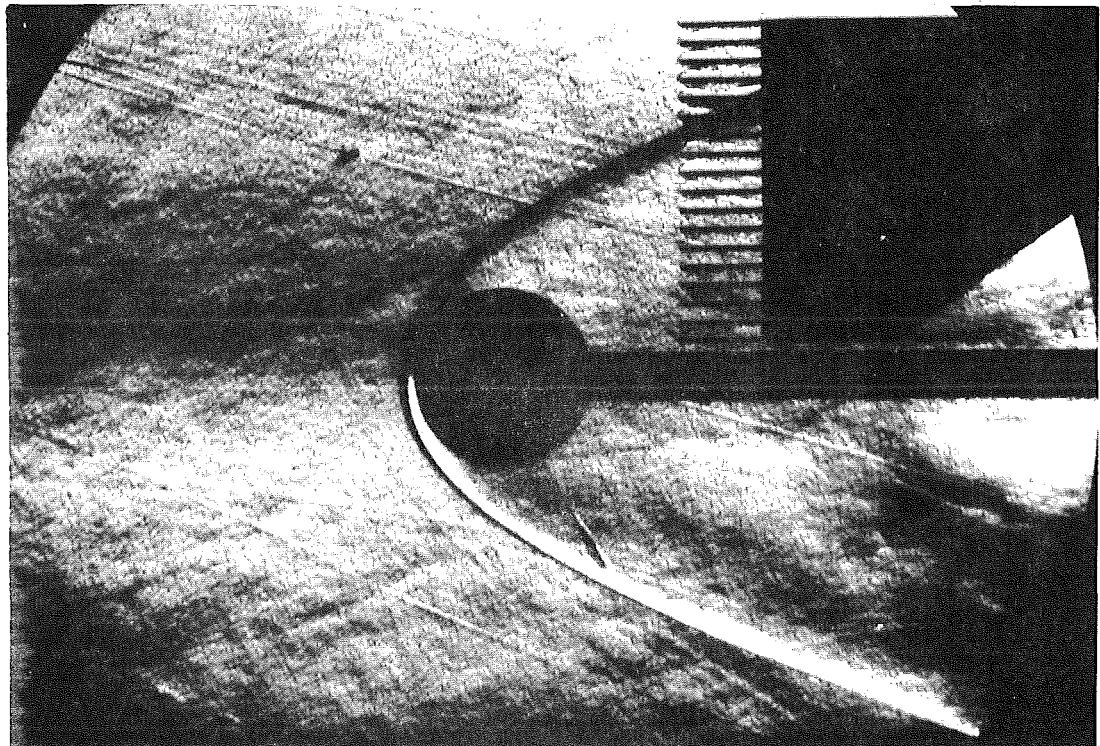


FIG 22. SCHLIEREN PHOTOGRAPH OF 1.6 INCH DIAMETER SPHERE
AT $M_{\infty} = 5.01$; WAKE TOTAL PRESSURE RAKE AT $X/D = 0.5$.

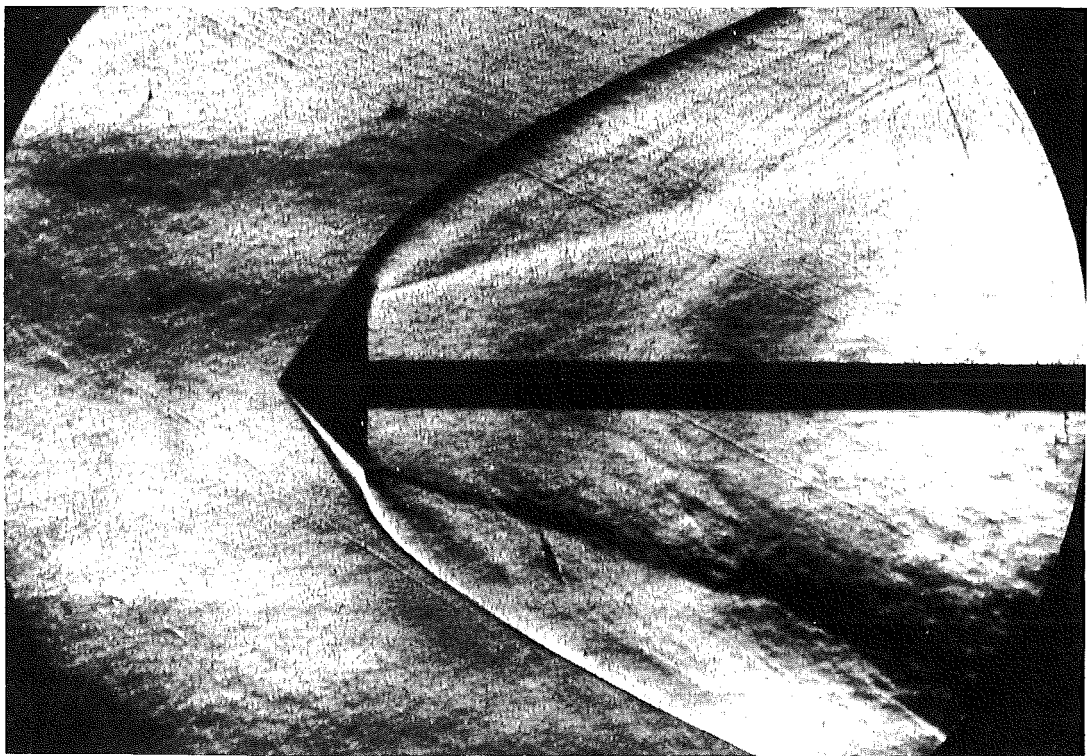


FIG 23. SCHLIEREN PHOTOGRAPH OF 1.6 INCH DIAMETER 45° HALF-ANGLE CONE AT $M_{\infty} = 4.01$ (SEPARATED FLOW IN BASE REGION); WAKE TOTAL PRESSURE RAKE AT $X/D = 4.46$.

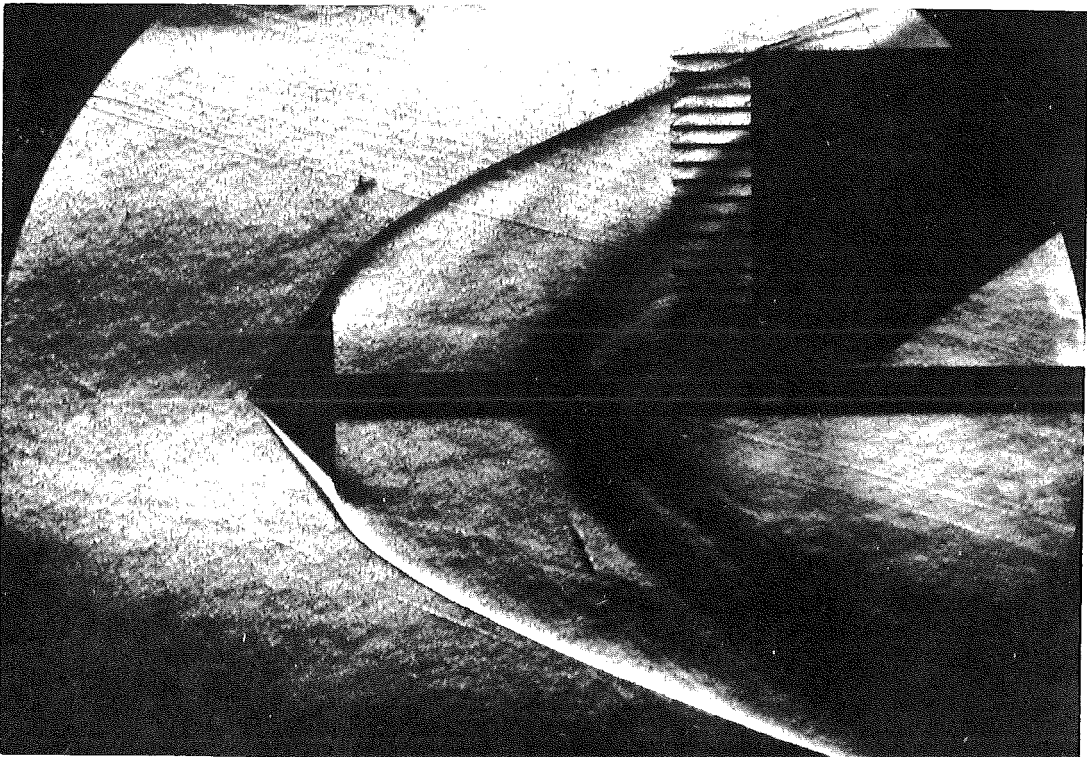


FIG 24. SCHLIEREN PHOTOGRAPH OF 1.6 INCH DIAMETER 45° HALF-ANGLE CONE AT $M_{\infty} = 5.01$; WAKE TOTAL PRESSURE RAKE AT $X/D = 2.0$.

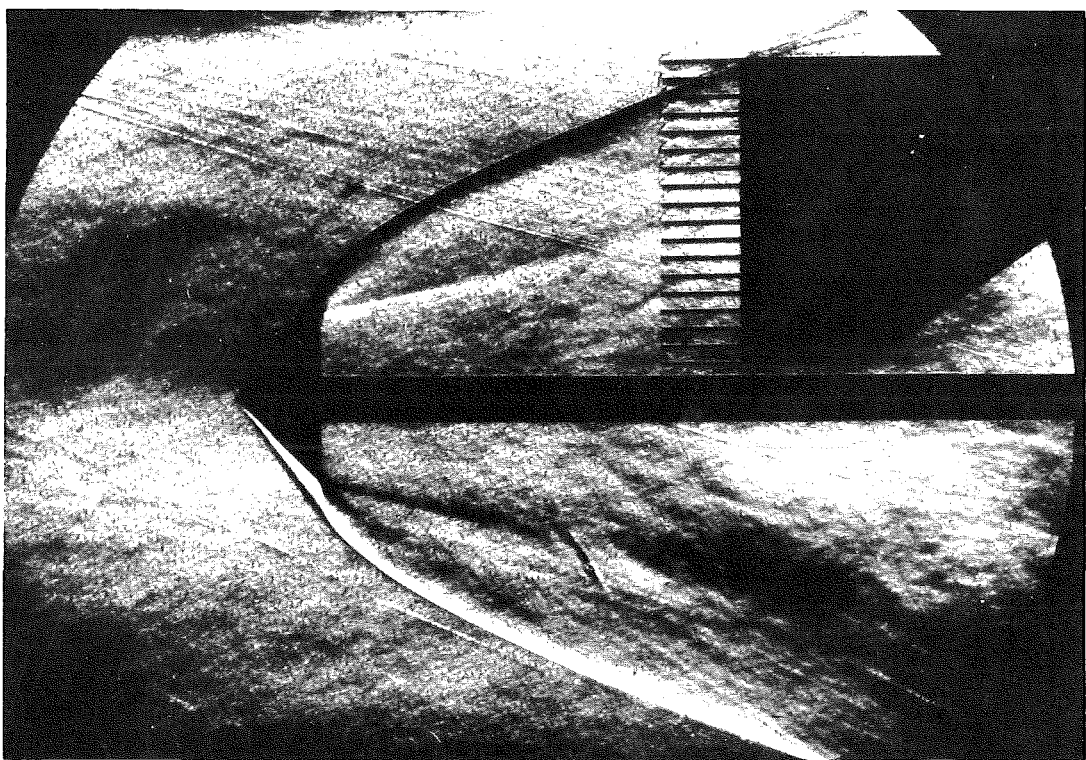


FIG 25. SCHLIEREN PHOTOGRAPH OF 1.6 INCH DIAMETER 45° HALF-ANGLE CONE AT $M_{\infty} = 5.01$ (SEPARATED FLOW IN BASE REGION); WAKE TOTAL PRESSURE RAKE AT $X/D = 2.0$.

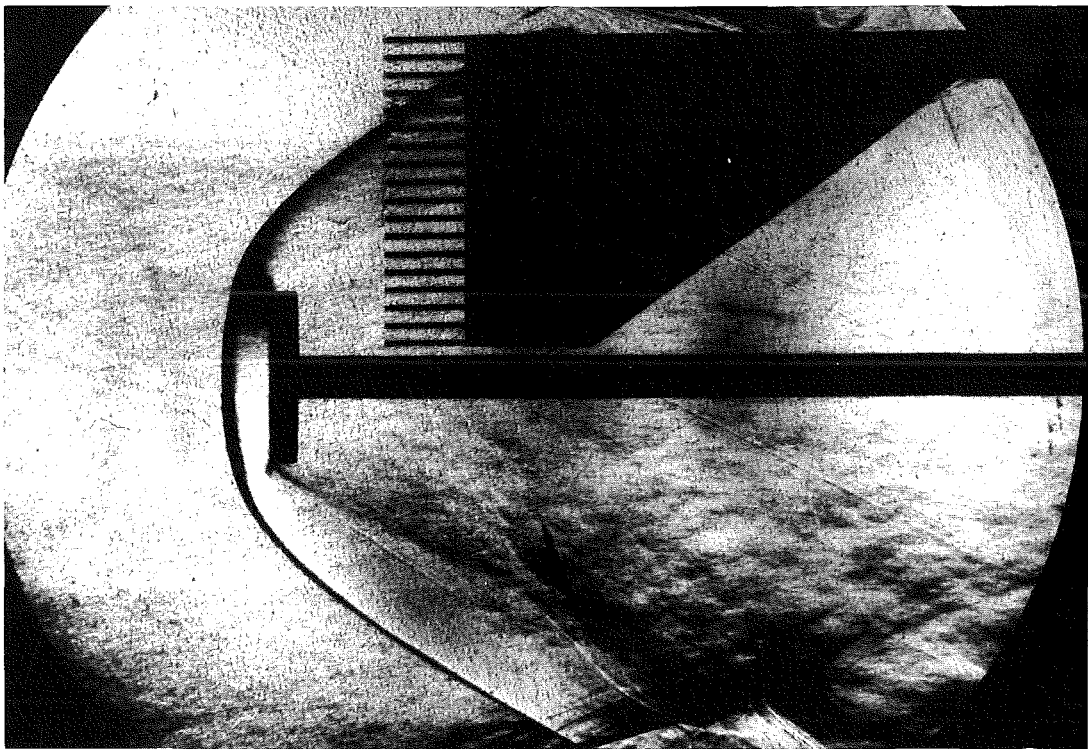


FIG 26. SCHLIEREN PHOTOGRAPH OF 1.6 INCH DIAMETER CIRCULAR FLAT PLATE AT $M_{\infty} = 4.01$ (SEPARATED FLOW IN BASE REGION); WAKE TOTAL PRESSURE RAKE AT $X/D = 0.5$.

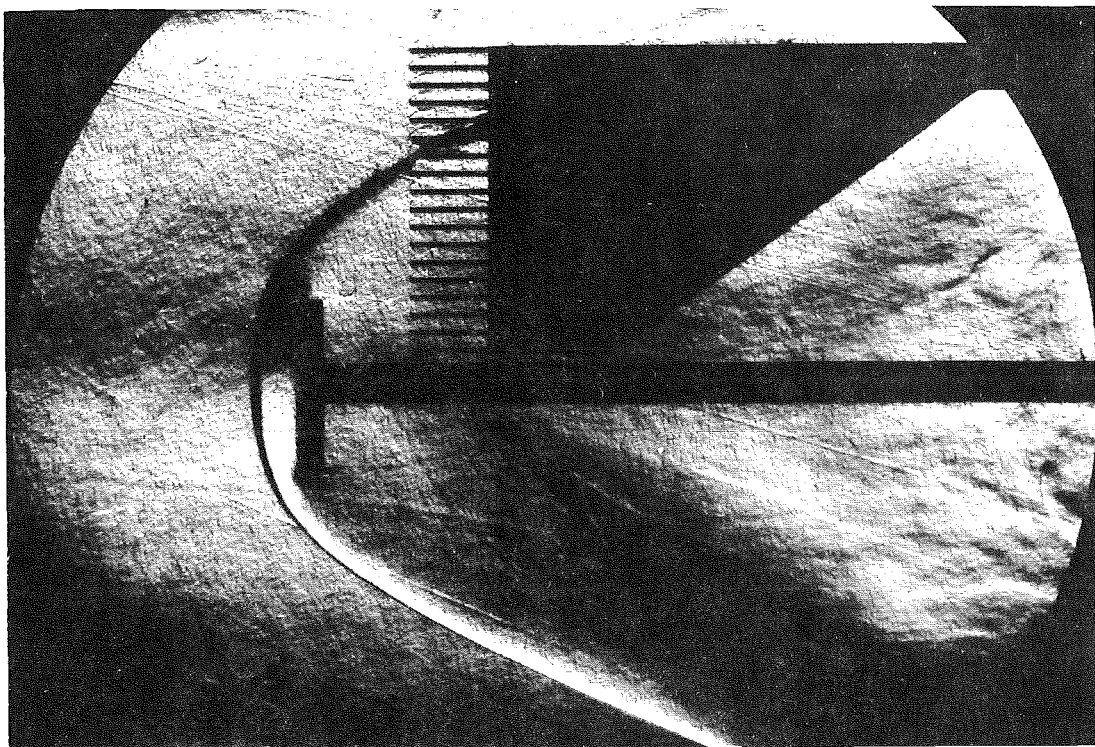


FIG 27. SCHLIEREN PHOTOGRAPH OF 1.6 INCH DIAMETER CIRCULAR FLAT PLATE AT $M_{\infty} = 5.01$; WAKE TOTAL PRESSURE RAKE AT $X/D = 0.5$.

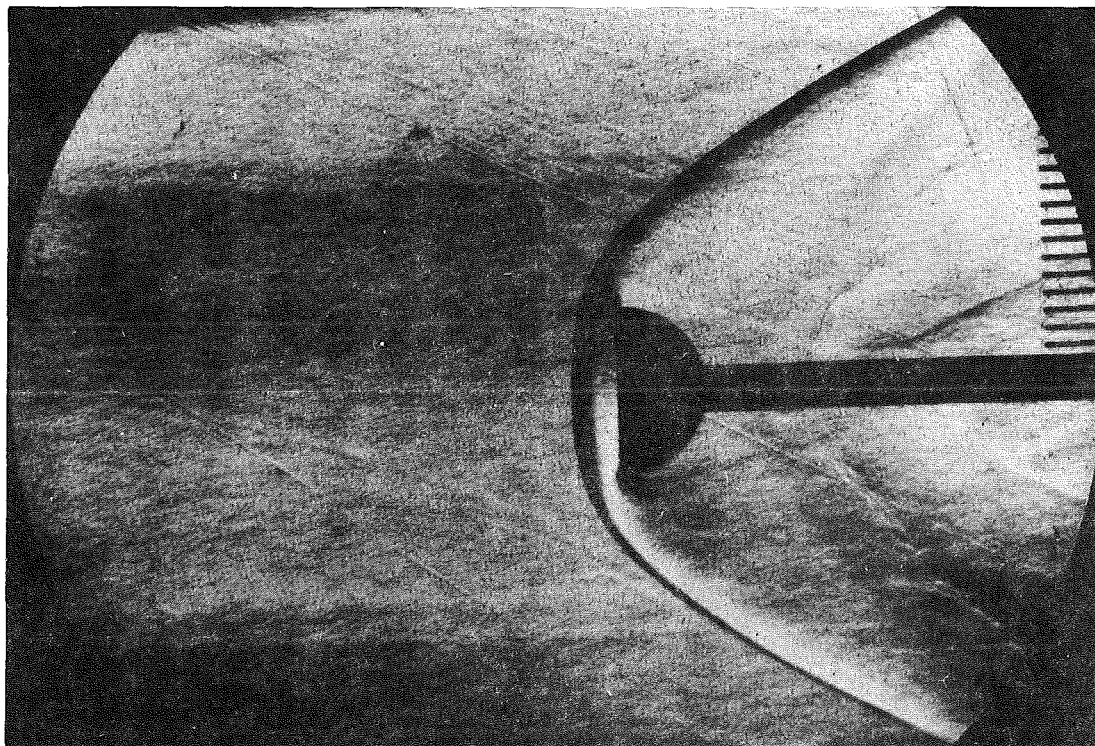


FIG 28. SCHLIEREN PHOTOGRAPH OF 1.6 INCH DIAMETER HOLLOW HEMISPHERE AT $M_{\infty} = 4.01$; WAKE TOTAL PRESSURE RAKE AT $X/D = 2.0$.

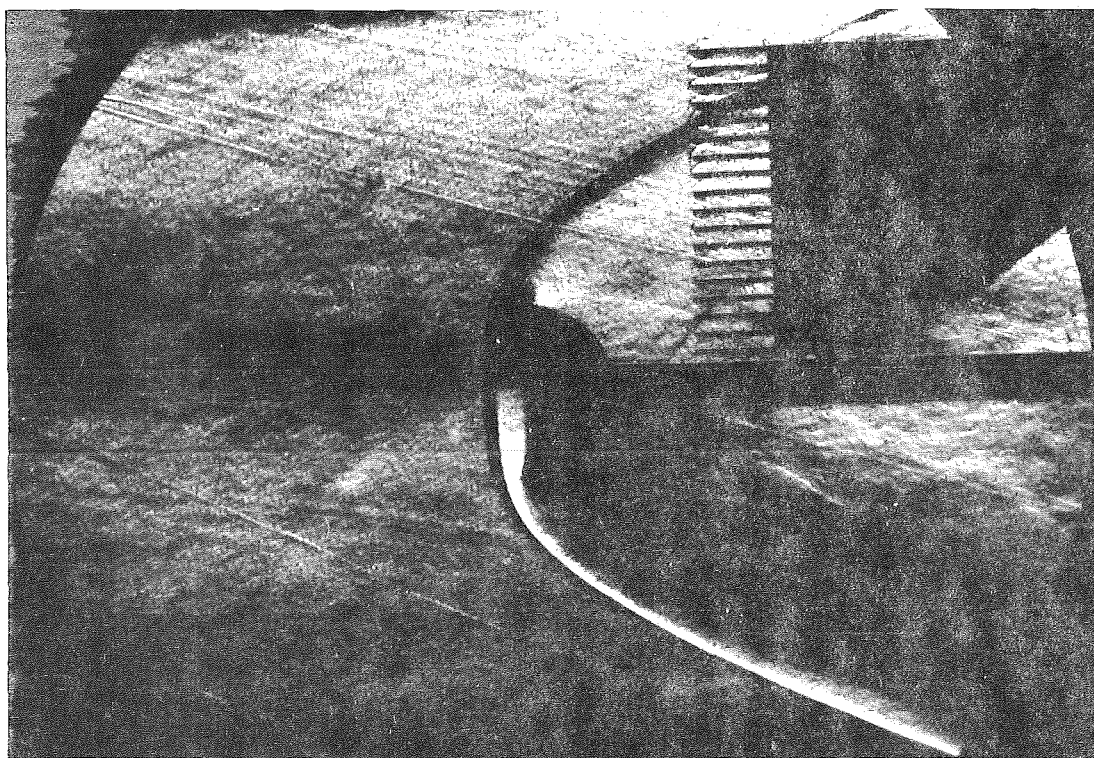


FIG 29. SCHLIEREN PHOTOGRAPH OF 1.6 INCH DIAMETER HOLLOW HEMISPHERE AT $M_{\infty} = 5.01$; WAKE TOTAL PRESSURE RAKE AT $X/D = 0.5$.

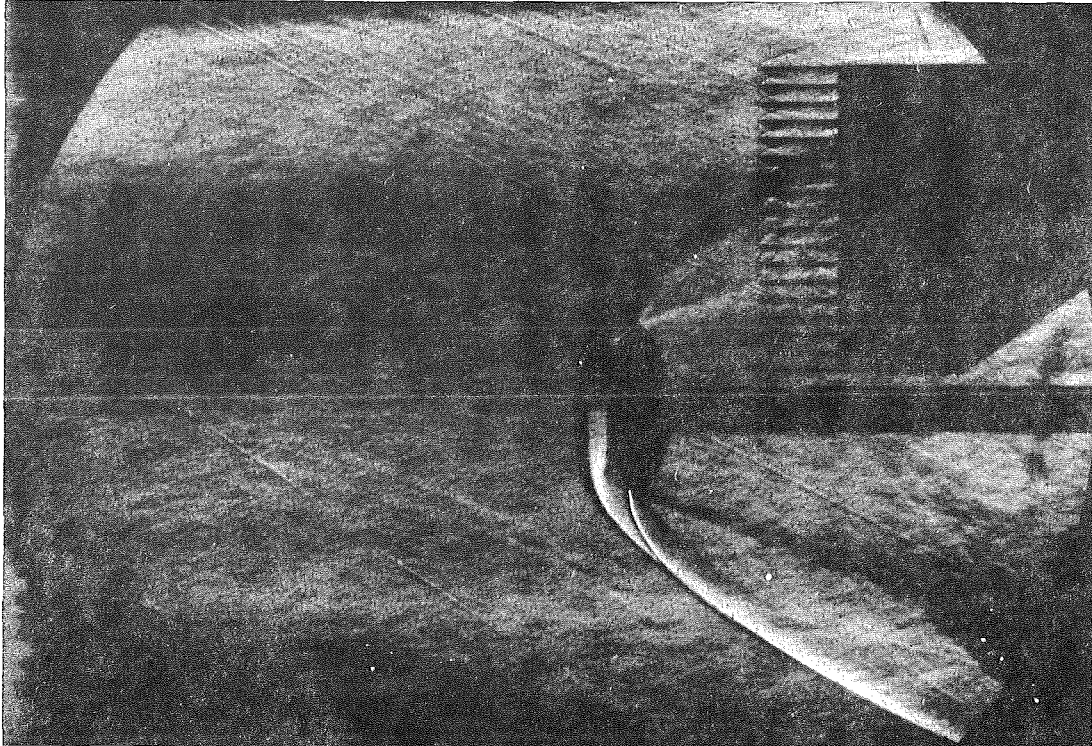


FIG 30. SCHLIEREN PHOTOGRAPH OF 1.6 INCH DIAMETER GUIDE SURFACE PARACHUTE MODEL AT $M_{\infty} = 4.01$ (SEPARATED FLOW IN BASE REGION); WAKE TOTAL PRESSURE RAKE AT $X/D = 0.5$.

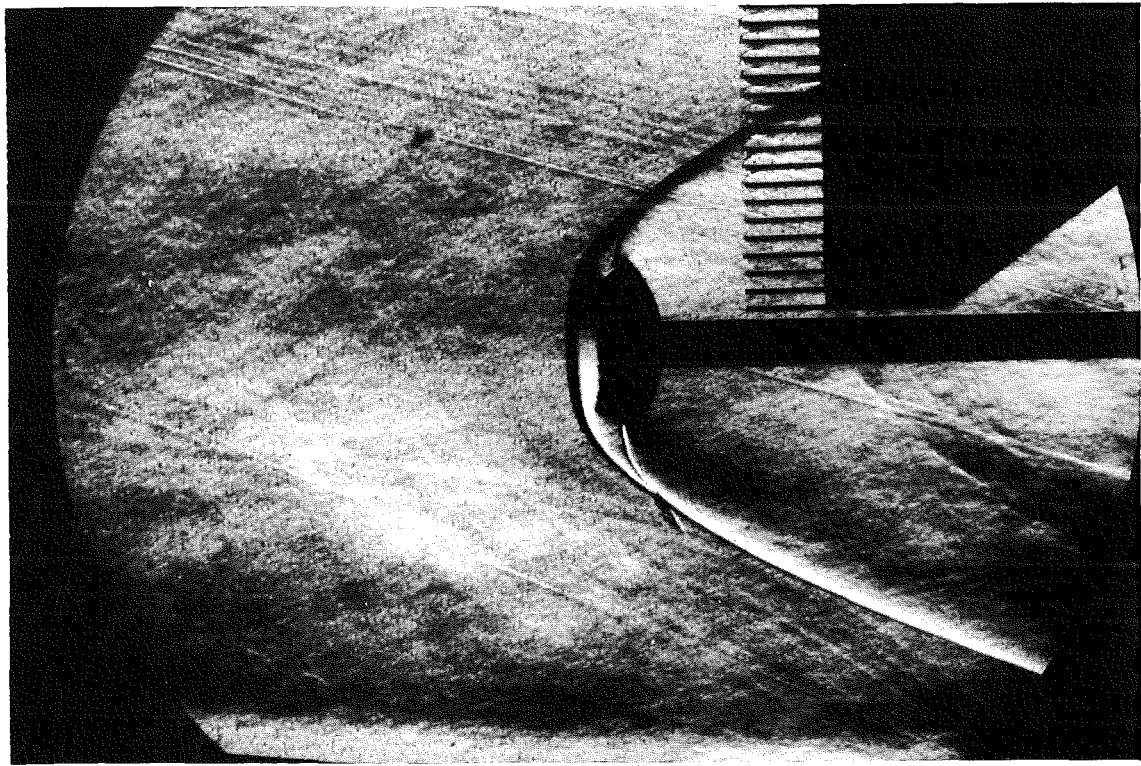


FIG 31. SCHLIEREN PHOTOGRAPH OF 1.6 INCH DIAMETER GUIDE SURFACE PARACHUTE MODEL AT $M_{\infty} = 5.01$; WAKE TOTAL PRESSURE RAKE AT $X/D = 0.5$.

APPENDIX II
TEST DATA

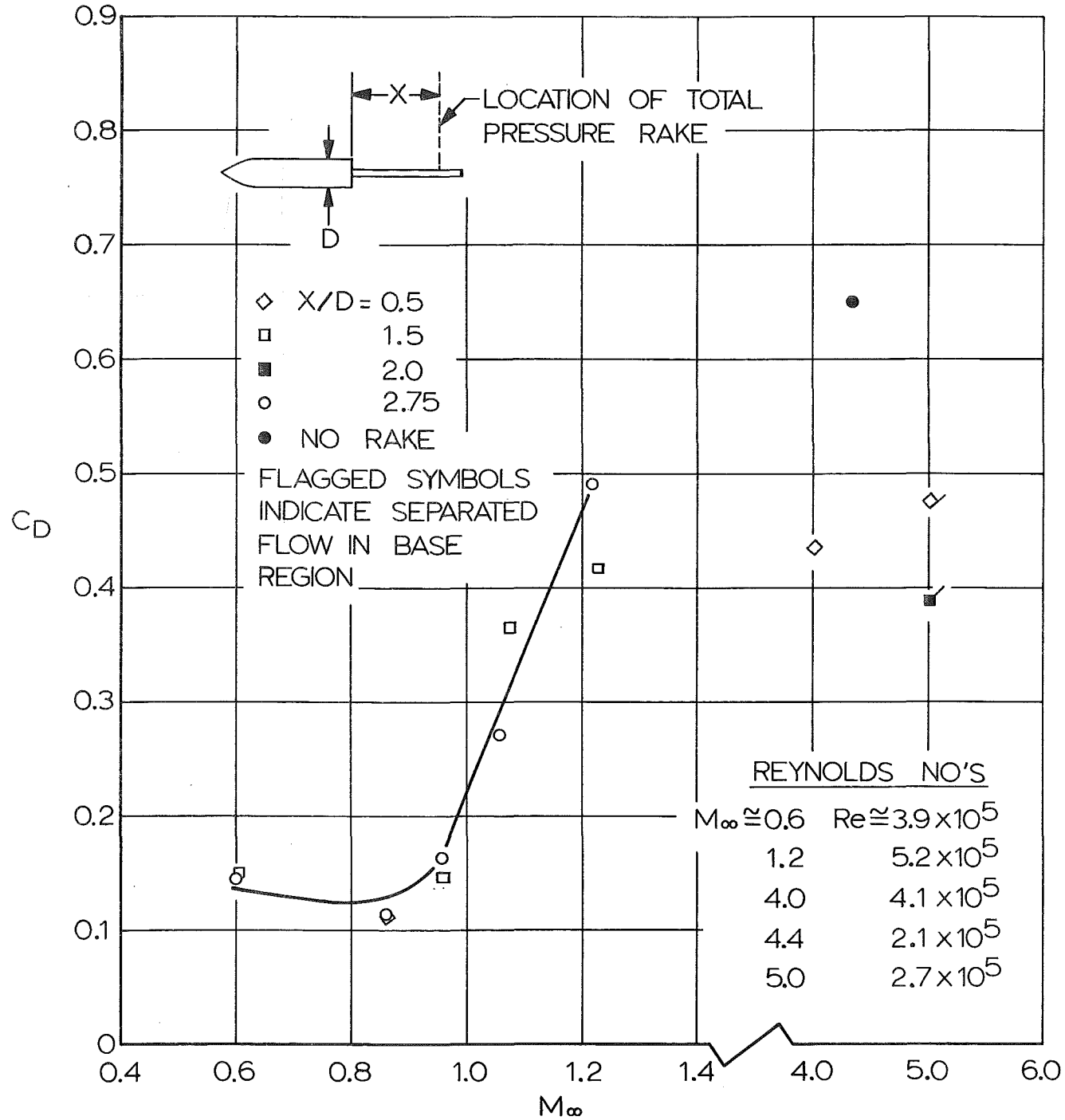


FIG 32. VARIATION OF DRAG COEFFICIENT OF OGIVE CYLINDER WITH FREE-STREAM MACH NUMBER

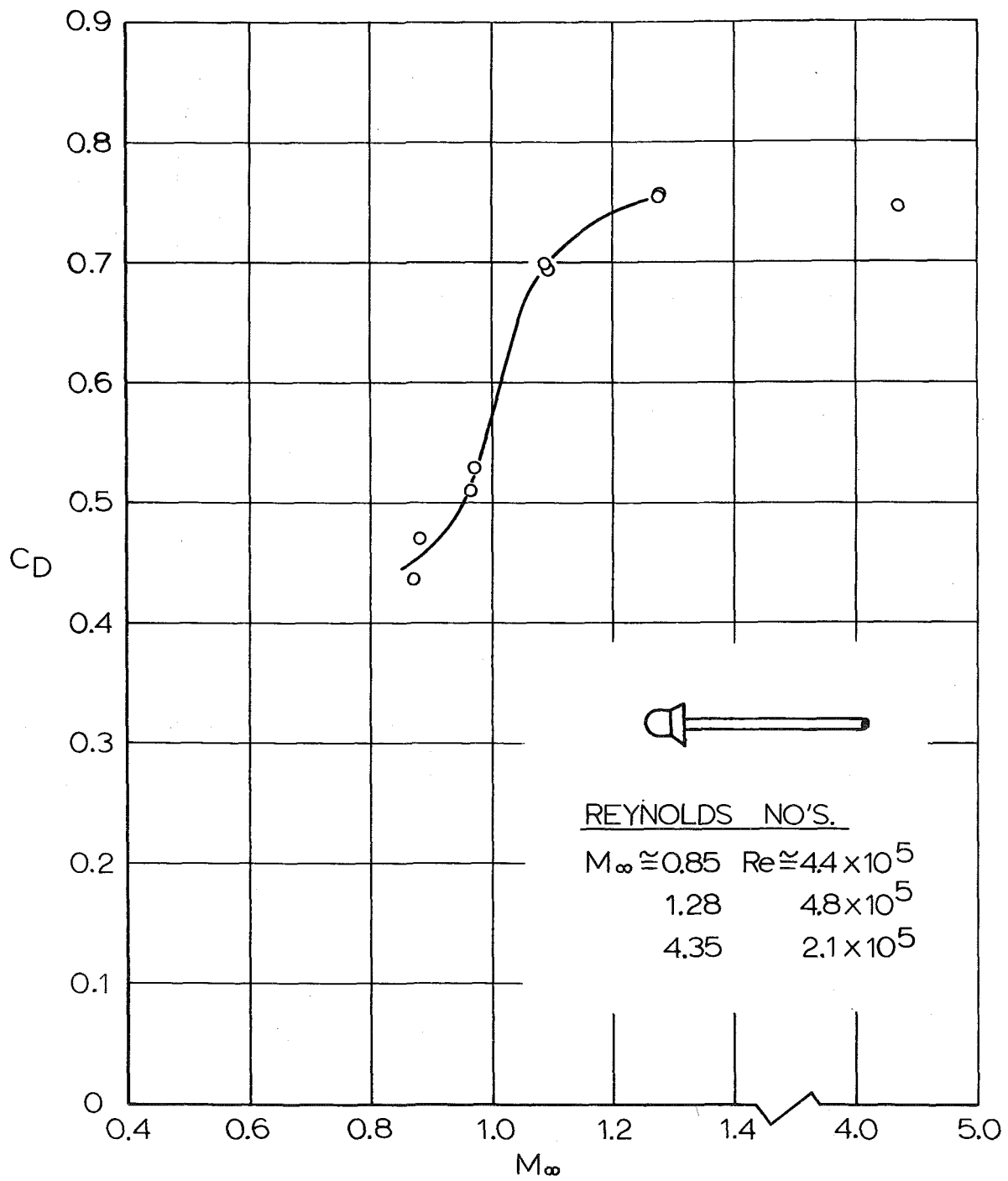


FIG 33. VARIATION OF DRAG COEFFICIENT OF SKIRTED HEMISPHERE WITH FREE-STREAM MACH NUMBER

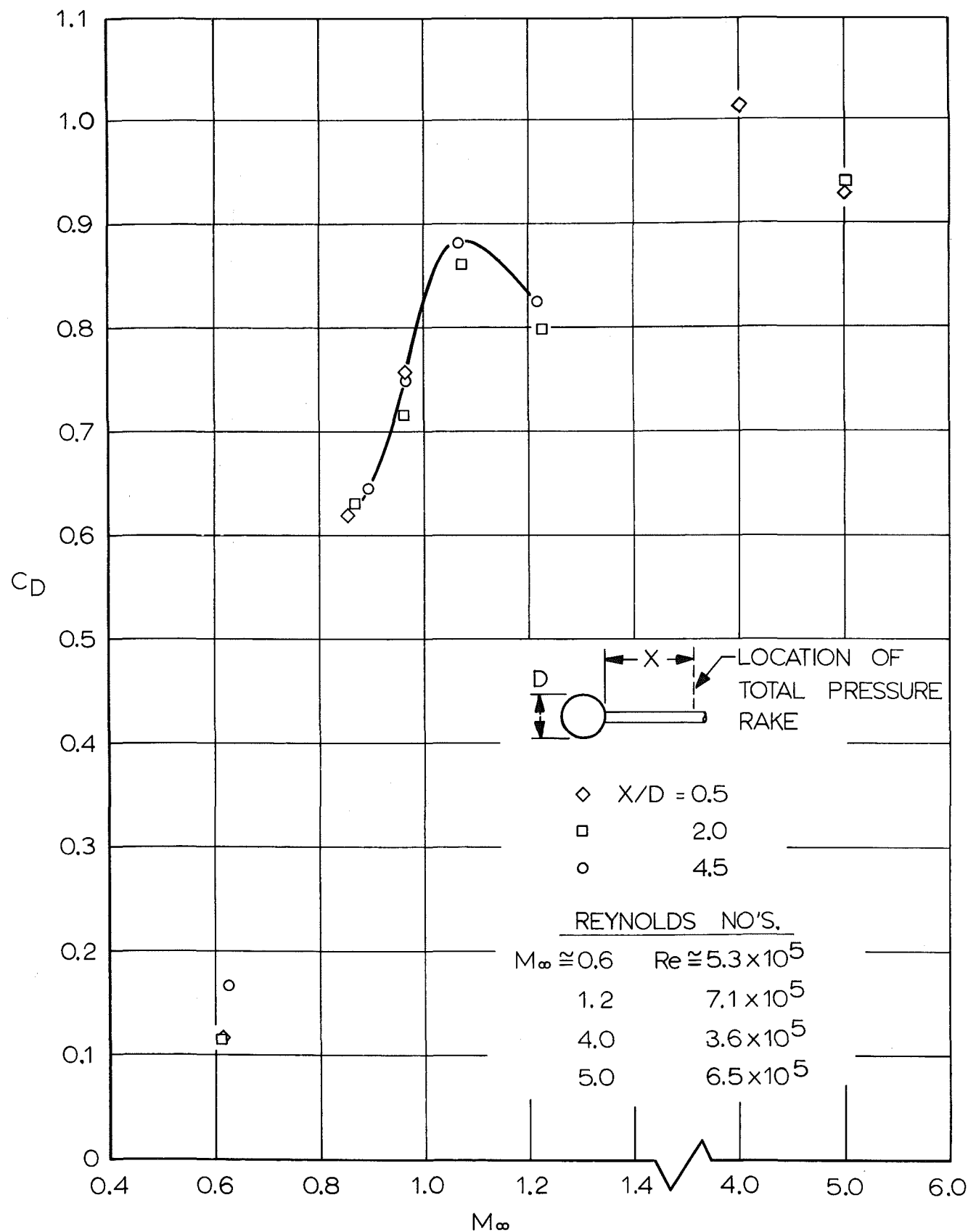


FIG 34. VARIATION OF DRAG COEFFICIENT OF SPHERE WITH FREE-STREAM MACH NUMBER

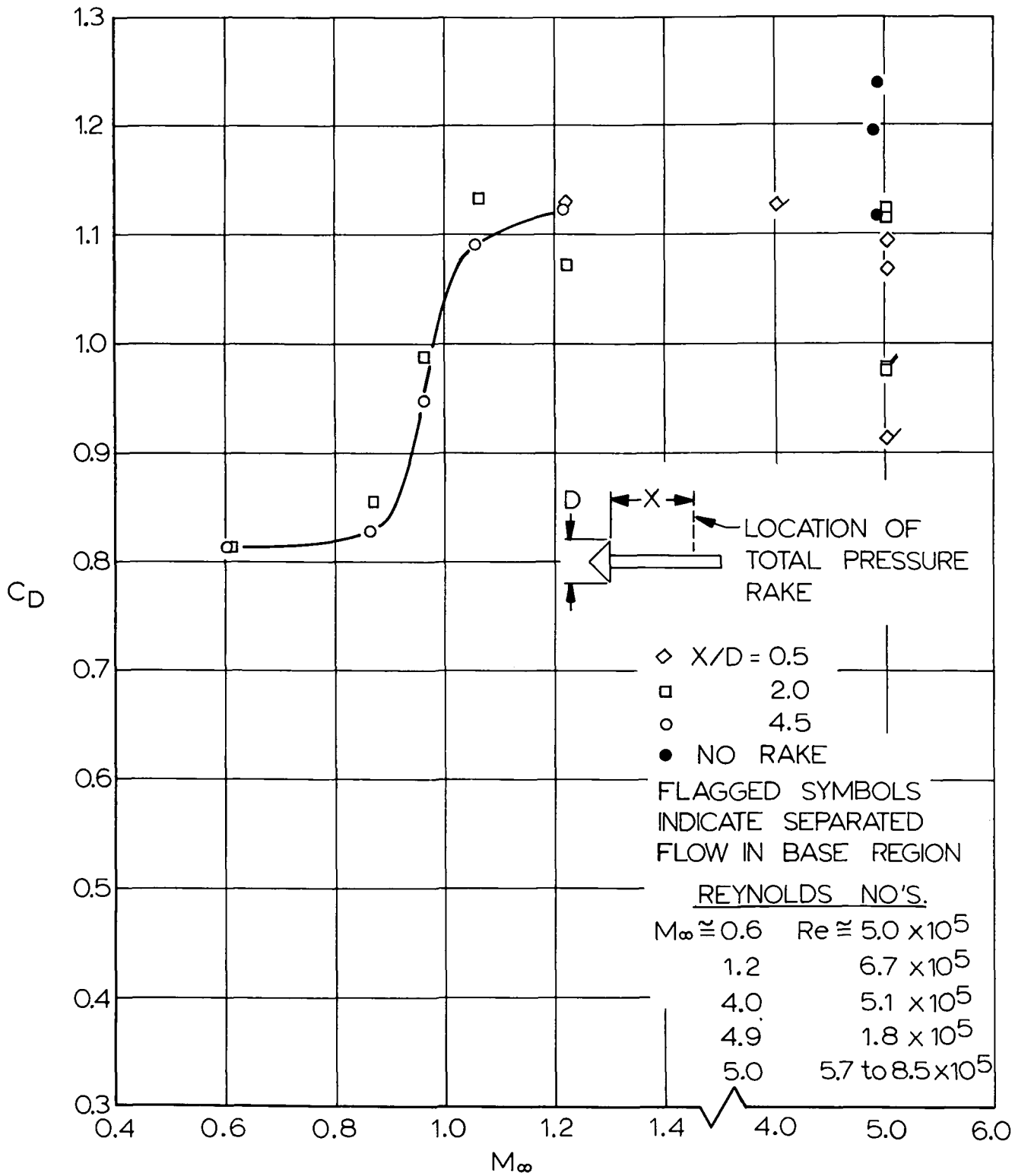


FIG 35. VARIATION OF DRAG COEFFICIENT OF
45° HALF-ANGLE CONE WITH FREE-
STREAM MACH NUMBER

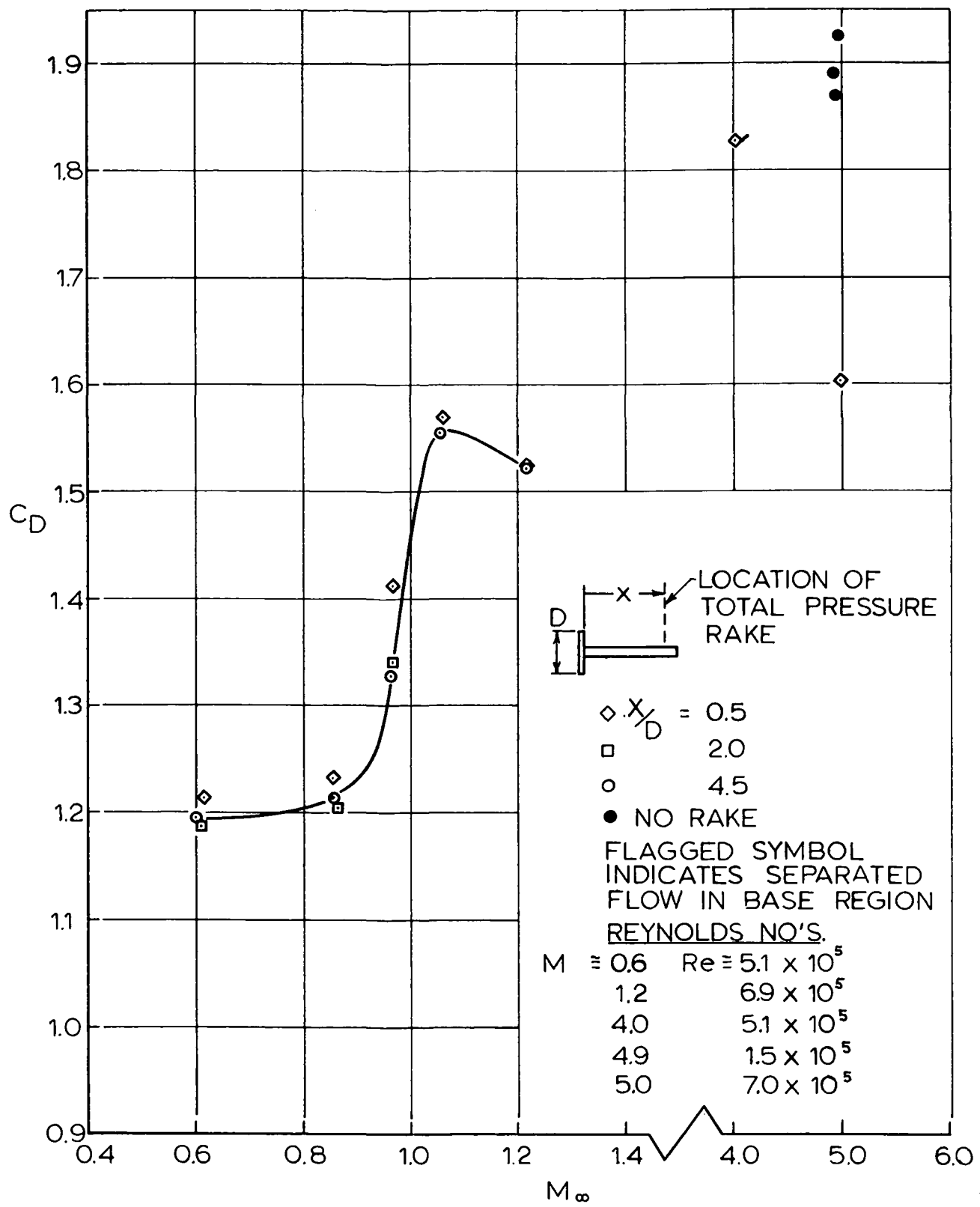


FIG 36. VARIATION OF DRAG COEFFICIENT OF CIRCULAR FLAT PLATE WITH FREE-STREAM MACH NUMBER

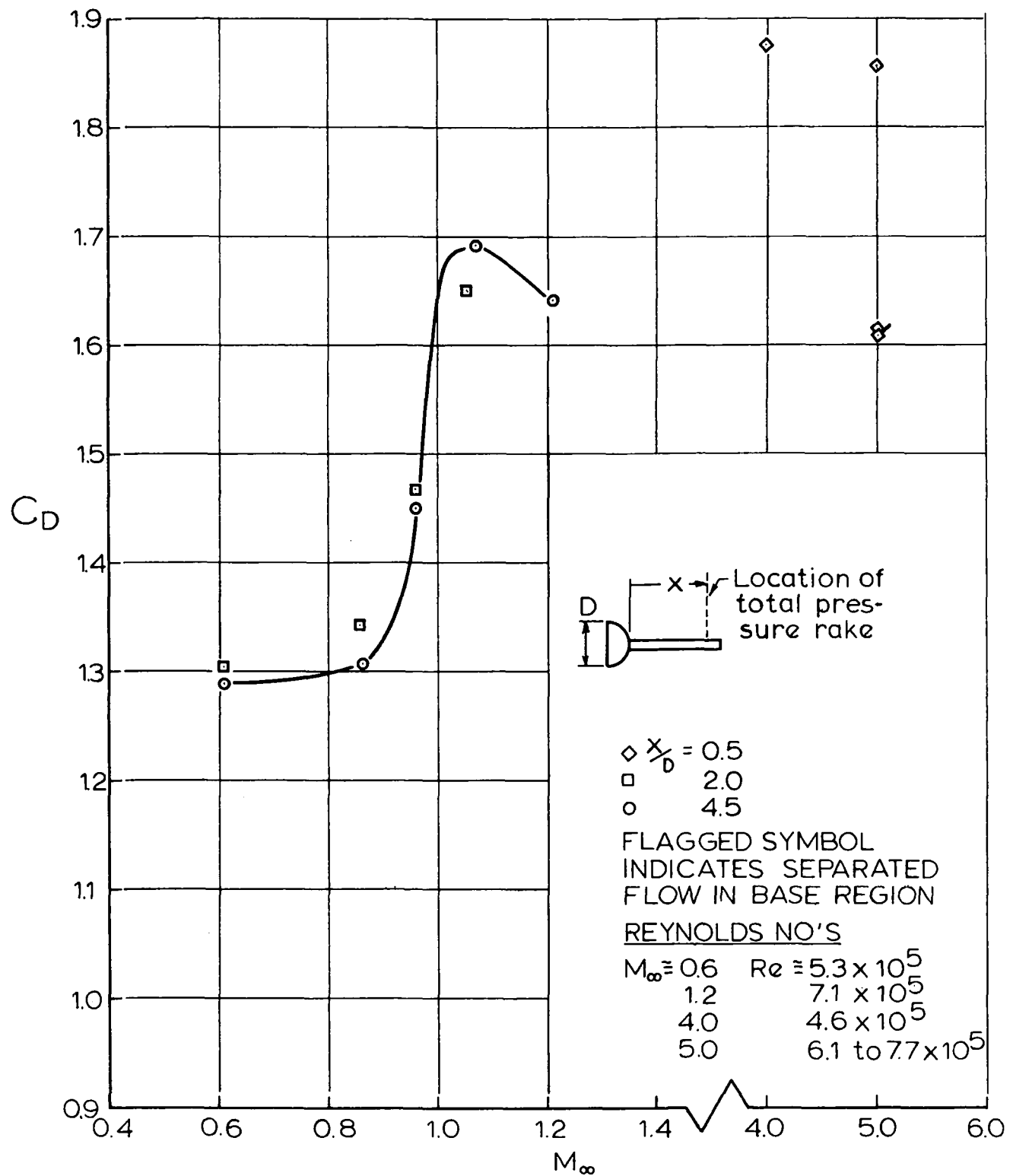


FIG. 37. VARIATION OF DRAG COEFFICIENT OF HOLLOW HEMISPHERE WITH FREE - STREAM MACH NUMBER

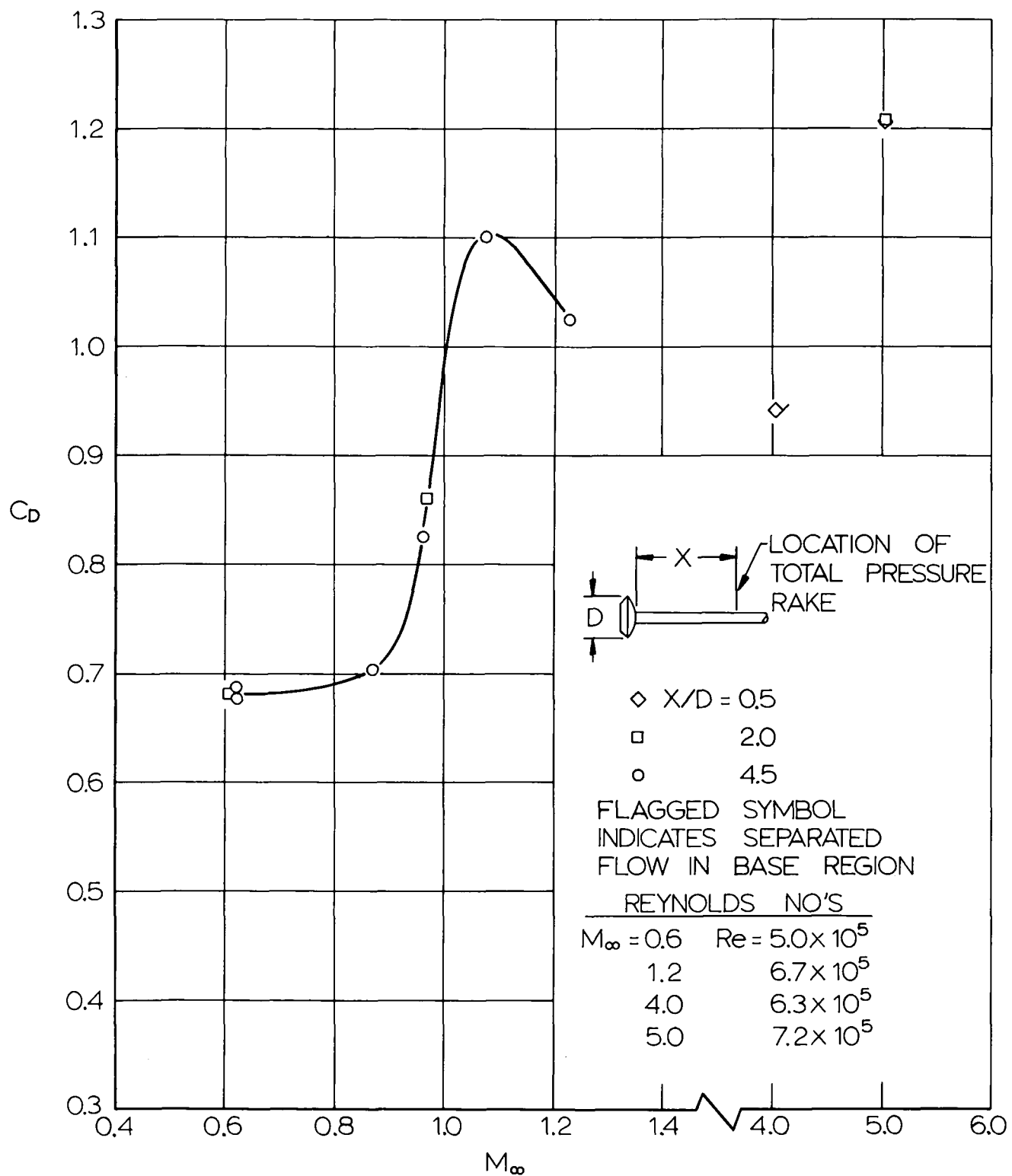


FIG 38. VARIATION OF DRAG COEFFICIENT OF GUIDE SURFACE PARACHUTE MODEL WITH FREE -STREAM MACH NUMBER 38

APPENDIX III

DESCRIPTION OF DRAG BALANCE SYSTEM

The drag balance system includes the balance (the mechanical portion of the system) and the associated electronic instrumentation. The balance, an exploded view is given in Fig 39, is composed of two primary parts, the main body and the drag sensing capsule. The electronic instrumentation consists of the drag sensing and calibration transformers, a signal generator, a control unit, and a recording unit.

The main body of the balance, which is 2.05 inches long and 1.554 inches in diameter, forms the fixed component of the balance and is rigidly attached to the balance support sting. In it is housed the drag sensing transformer and its positioner and also an internal pressure tap and thermocouple. The Schaevitz Linear Variable Differential Transformer (Type OLOM-L) is attached to the upstream end of its positioner. The other end of the positioner is spring loaded against a cam, rotation of which provides axial positioning of the transformer.

The drag sensing capsule, which is 3.102 inches long and 1.554 inches in diameter, is composed of a fixed inner shell and a floating outer shell. The two shells are coaxially arranged and are connected together by two ring-type steel diaphragms which provide the spring force for drag sensing. The inner shell slides onto the inner tube of the main body and is rigidly attached to the main body by a rod which provides adjustment of the width of the slot between the main body and outer shell of the drag sensing capsule.

The outer shell, which is thus free to deflect the diaphragms, forms the drag sensing element. The transformer core is attached to its downstream end and the test model sting is rigidly attached by means of an adapter to the upstream end.

A drag force on the test model causes an axial displacement of the outer shell of the drag sensing capsule

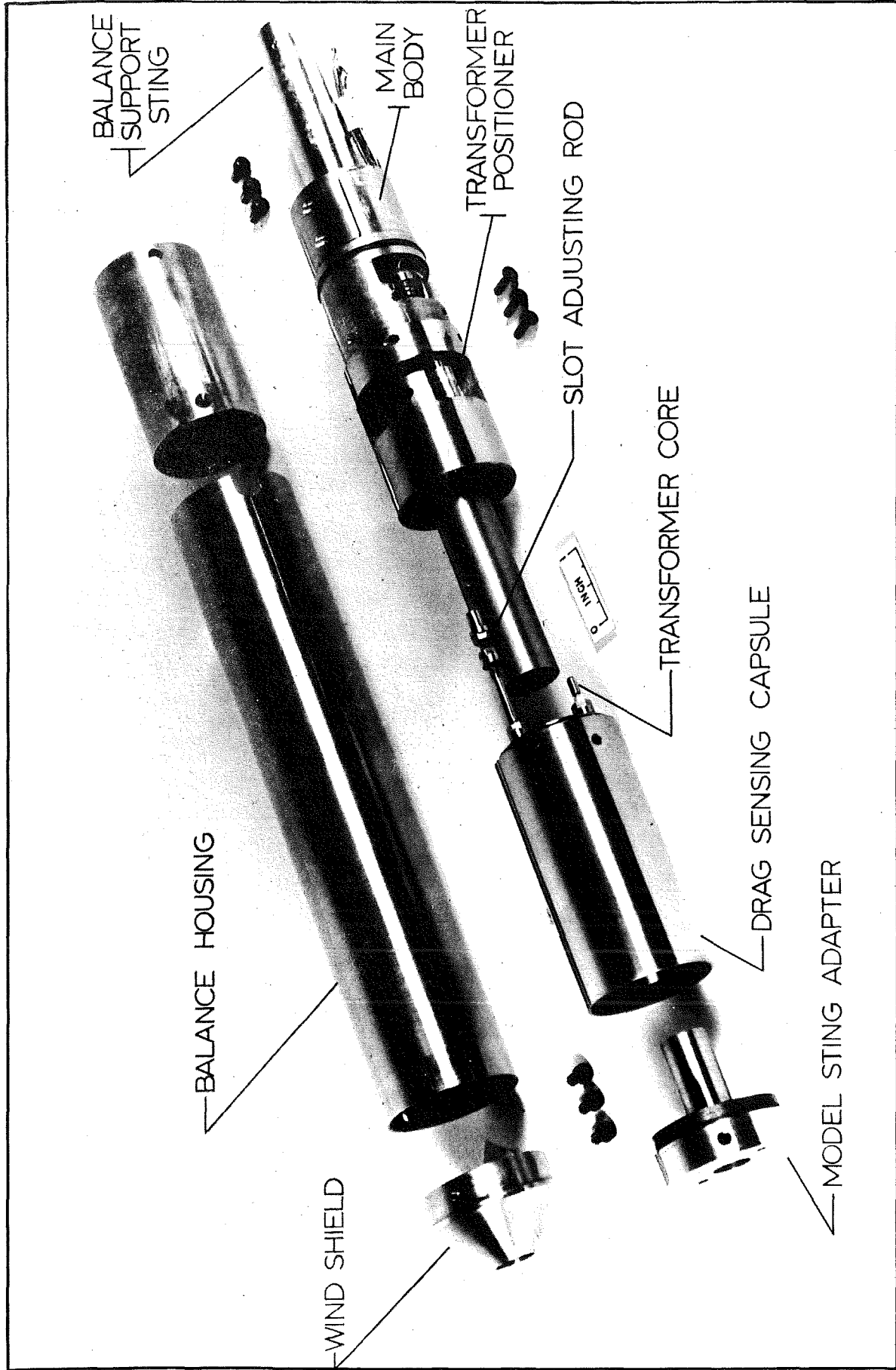


FIG 39. DRAG BALANCE

relative to the fixed main body. This displacement, which is proportional to the drag on the model, is measured by the Schaevitz LVDT. The LVDT is energized by a 10 KC signal generator and its output is transmitted to a Brown Variable Span Recorder through the control unit. Since the output of the signal generator to the LVDT must be constant, the generator is voltage regulated and is located in a sound proofed room to isolate it from tunnel noise.

As a displacement of the outer shell of the drag sensing capsule causes an equal displacement of the transformer, the transformer gives an output which is proportional to the drag. The control unit converts this output into useful recorder information and also extends the recorder range, thereby permitting measurement of drag over a wide range without loss of sensitivity. Two other LVDT's, a "Hi" and a "Lo" at different points on the scale, are used as calibration transformers. They provide a continuous check on the accuracy of the system and minimize errors due to temperature fluctuations.

A linear variation of transformer output with drag, good sensitivity, and excellent zero return are obtained.

LIST OF REFERENCES

1. Heinrich, H. G. and Haak, E. L.: The Drag of Cones, Plates, and Hemispheres in the Wake of a Forebody in Subsonic Flow, ASD TR 61-587, December, 1961.
2. Aeronautical Research Facilities, University of Minnesota, Institute of Technology, Department of Aeronautical Engineering, Rosemount Aeronautical Laboratories, Research Report No. 132, 1956.
3. Hoerner, S. F.: Fluid Dynamic Drag, published by author, Midland Park, New Jersey, 1958.
4. Charter's A. C. and Thomas, R. N.: The Aerodynamic Performance of Small Spheres from Subsonic to High Supersonic Velocities, Journal of the Aeronautical Sciences, Vol. 12, No. 4, pp. 468-476, October, 1945.
5. Hodges: The Drag Coefficient of Very High Velocity Spheres, New Mexico School of Mines /RDD/T-656, 1949.
6. May, A. and Witt, W.: Free Flight Determinations of the Drag Coefficient of Spheres, US Naval Ordnance Laboratory, Report No. 2352, 1952.
7. Kane, E. D.: Sphere Drag at Supersonic Speeds and Low Reynolds Numbers, Journal of the Aeronautical Sciences, Vol. 18, No. 4, pp. 259-270, April, 1951.
8. Sphere Drag in Rarefied Supersonic Gas Flows, Jet Propulsion Laboratory, Research Summary No. 36-5, Vol. II, pp. 10-11, November 1, 1960.
9. Ashkenas, H. I.: Sphere Drag at Low Reynolds Numbers and Supersonic Speeds, Jet Propulsion Laboratory, Research Summary No. 36-12, Vol. I, pp. 93-96, January 2, 1962.
10. Johnston: An Investigation of the Flow About Cones and Wedges at and beyond the Critical Angle, University of Toronto, Institute of Aerophysics, Report No. 24, 1952.
11. Drougge: The Flow Around Conical Tips in the Upper Transonic Range, Aeronautical Research Institute of Sweden, Report No. 25, 1948.
12. The Effect of Nose Shape on Missile Nose Drag, Rosemount Aeronautical Laboratories, Research Report 55, 1950.

13. Stoney, W. E., Jr.: Collection of Zero-Lift Drag Data on Bodies of Revolution from Free Flight Investigations, NACA TN 4201, January, 1958.
14. Walchner, O.: Systematic Wind Tunnel Measurements on Missiles, NACA TM 1122, March, 1947.
15. Ferri, A.: Supersonic Tunnel Tests of Projectiles in Germany and Italy, NACA ACR No. L5H08, October, 1945.